

---

# Data-Error Scaling in Machine Learning on Natural Discrete Combinatorial Mutation-prone Sets: Case Studies on Peptides and Small Molecules

---

Vanni Doffini<sup>1,2,3,\*</sup> O. Anatole Von Lilienfeld<sup>4,5,6</sup> Michael A. Nash<sup>1,2,3,†</sup>  
<sup>1</sup>University of Basel <sup>2</sup>ETH Zurich <sup>3</sup>Swiss Nanoscience Institute  
<sup>4</sup>University of Toronto <sup>5</sup>Vector Institute <sup>6</sup>TU Berlin

## Abstract

We investigate trends in the data-error scaling behavior of machine learning (ML) models trained on discrete combinatorial spaces that are prone-to-mutation, such as proteins or organic small molecules. We trained and evaluated kernel ridge regression machines using variable amounts of computationally generated training data. Our synthetic datasets comprise i) two naïve functions based on many-body theory; ii) binding energy estimates between a protein and a mutagenised peptide; and iii) solvation energies of two 6-heavy atom structural graphs. In contrast to typical data-error scaling, our results showed discontinuous monotonic phase transitions during learning, observed as rapid drops in the test error at particular thresholds of training data. We observed two learning regimes, which we call saturated and asymptotic decay, and found that they are conditioned by the level of complexity (i.e. number of mutations) enclosed in the training set. We show that during training on this class of problems, the predictions were clustered by the ML models employed in the calibration plots. Furthermore, we present an alternative strategy to normalize learning curves (LCs) and the concept of mutant based shuffling. This work has implications for machine learning on mutagenisable discrete spaces such as chemical properties or protein phenotype prediction, and improves basic understanding of concepts in statistical learning theory.

## 1 Introduction

Machine learning (ML) has garnered significant interest in recent years, particularly with the release of generative models such as BERT [20], (Chat-)GPT [46], Gemini [69], LLaMA [72, 73], Mistral [32], DALL-E [53, 54, 10], and Stable Diffusion [57, 62] to the general public. Similarly, the introduction of AlphaFold [64, 34] represented a turning point in protein science [78, 39], providing researchers with the ability to predict 3D structures [41, 6] of single proteins or even protein complexes from primary sequences [23]. Nevertheless, predicting the effects of mutations on protein phenotype [15] is a monumentally challenging task [11, 49] due to the complexity of the problem (epistasis) [14, 86], the wide range of protein phenotypes of potential interest, and the dearth and cost of high-quality training data.

One meaningful difference in this context exists between global (e.g., de-novo protein design, AlphaFold structure prediction) and local (e.g., variant libraries, directed evolution) optimization [45]. For global optimization, a large number of diverse proteins need to be cataloged, annotated or labeled. In contrast, for local optimization a combinatorially large number of mutant sequences (Fig. 1) with high similarity to a single parent sequence (wild-type, WT) must be screened and assigned phenotype

---

\*vanni.doffini@unibas.ch

†michael.nash@unibas.ch

values. Even with state-of-the-art experimental techniques such as high-throughput screening [27, 24], next generation sequencing (NGS) [71, 59] and deep-mutational scanning (DMS) [75, 76, 33], or automated laboratories [55, 61], the fraction of variants that can be analyzed is miniscule compared to the size of potentially interesting sequence space.

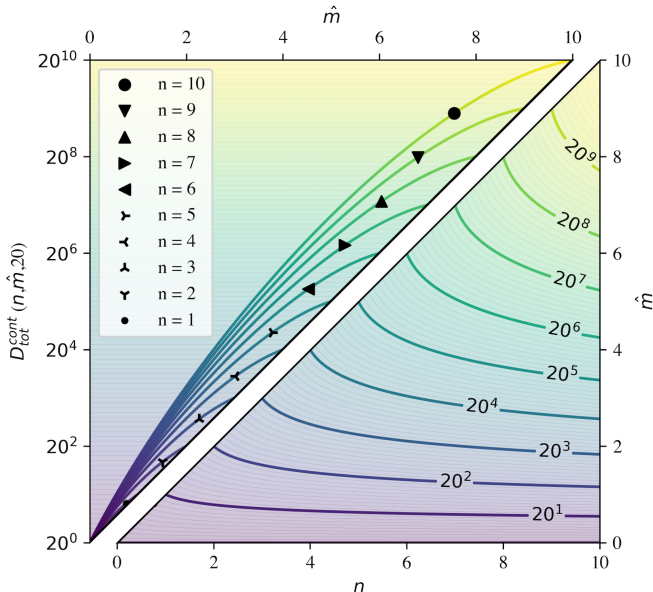


Figure 1: Size of cumulative combinatorial space for a linear graph (e.g., a peptide). The number of cumulative combinations ( $D_{tot}^{cont}$ ) is shown while changing the length of the linear graph ( $n$ , number of amino acids in chain) and the number of mutations in the sequence ( $\hat{m}$ ). The vocabulary size was kept constant (20).

De-novo protein design is broader but coarser, while mutant-based design is task-specific and less generalizable. Nevertheless, scientists have successfully implemented ML for both tasks, generating new proteins [5, 88] and enhancing the biological fitness of variants derived from parent sequences [28, 25, 14, 82]. The latter has been especially useful for enhancing directed evolution [84, 85, 12, 70], an experimental approach where specific traits are enhanced through iterative screening/selection and enrichment of variant sequences possessing beneficial mutations [58, 87].

To validate ML-based approaches in protein and molecular engineering, it is important to evaluate how quickly a given model is able to learn a given task. This allows comparisons of performance and efficiency to be made between various models. The learning rate depends on several parameters, such as the architecture (complexity) of the model, how data are encoded, if feature engineering is employed as well as how the cost of model training scales with input data size.

One important tool to study, compare and extrapolate the learning process of ML models is the so-called learning curve (LC) [44, 65, 4], which is a subset of the neural scaling law concept [68, 26, 7, 35, 66]. LCs were introduced in the statistical mechanics field [22, 47, 83, 67] and recently popularized in computational chemistry and physics to assess predictions of quantum machine learning (QML) tasks [80, 30]. The main concept is to train a model consisting of a particular architecture, data structuring, or algorithm by feeding it increasing fractions of the total available training data. For each training instance, a performance metric on an independent and constant (test) dataset is evaluated. Scaling in LCs can usually be modelled as a power law with an offset [79, 18], according to

$$\epsilon_{test} = a(N_{train})^b + c \quad (1)$$

where the offset ( $c$ ) is related to the level of noise in the data,  $\epsilon_{test}$  represents the model error, and the parameters ( $a$ ) and ( $b$ ) describe the learning rate of the model. Fitting different architectures and

techniques result in different LCs, which can be compared to assess diverse ML models and decide which model presents better scalability. LCs can also be used to quantify if and how much additional data are necessary to reach a certain accuracy. Despite a strong desire in the community to understand on a deeper level how the ML process works, LCs are sparsely used outside theoretical fields.

In the case of protein phenotype prediction, the learning tasks are of a special kind. Protein sequence space is discrete, with a fixed set of typically 20 amino acids included in the mutational vocabulary of proteins. To the best of our knowledge, there has not been an in-depth study to understand how the combinatorial discreteness of protein sequence space could influence the shape and behavior of learning curves. A similar paradigm can also be applied to ML of small molecule properties where molecules can be ‘mutagenized’ by altering substituent groups, however, the mutational space can be further complicated by changes in topology of the backbone upon mutation.

To bridge this knowledge gap, we present a computational and theoretical study on the scaling behavior of LCs obtained during ML training on different restricted (bio-)chemical input spaces with deterministic fitness functions. Using our workflow (Fig. 2), we show that the expected LC trends cannot be described by single power laws, but exhibit periods of accelerated and decelerated learning, a behavior closely related to discontinuous learning [22, 79, 26, 67]. Such observation could be also related to the double-descent behaviour reported for modern neural networks [8]. Moreover, we show that the accelerations observed in the LCs emerge when training examples containing higher numbers of mutations are introduced or upon saturation and exhaustion of training examples containing a certain number of mutations in the training set. These findings could highly impact the way experiments and/or simulations are planned, how information-rich mutational data are most efficiently generated, and how they can be scaled. This is particularly relevant in biology, but can also be extended to other fields where discrete combinatorial prone-to-mutation input spaces are relevant.

## 2 Results and Discussion

### 2.1 Workflow Overview

We started by generating two databases containing all possible point mutations on three systems, consisting of a peptide and two small molecules. The systems were (1) Fg- $\beta$ , a peptide derived from a portion of the human fibrinogen beta chain (Fig. 2A); (2) hexane; and (3) cyclohexane. Although the term “mutation” is typically utilized for protein variants derived from a parent or WT sequence, here we extended this concept to organic small molecules by substituting one or more heavy atoms, carbon in our case, with nitrogen or oxygen, fixing the hybridization to Sp3 and filling with hydrogens. In contrast to the case with protein mutants where each point mutation is unique, for simple molecules this is not true due to symmetries. Such symmetric mutations can lead to duplicate entries in our molecule databases, however, for simplicity we left such duplicates in place.

We then used different functions to generate a set of response variables for each database entry. For the peptide variant database, we utilized two many-body based functions [81] and an estimator of the binding affinity (EvoEF) [50, 31] between the mutagenized peptide and its natural receptor, a protein called SdrG from *S. epidermidis* [52] (Fig. 3B). For the small molecules in the chemical database, we calculated the free energy of solvation in water at 298K using LeRuLi [21, 9, 17], which utilized the Abraham linear solvation energy relationship (LSER) [42, 2] and the Platts group additivity method [51].

We then converted each member in the database to a numerical value using standard one-hot-encoding (OHE, Fig. 2B). We used Laplacian kernel machines to learn the generated response variables from the OHE matrix using different numbers of training samples (Fig. 2C). The hyperparameter optimization ( $\sigma$ , kernel scale) was performed via grid search using as validation set a number of datapoints equal to the number of possible quadruple mutations. To test the performance, we used the mean absolute error (MAE) metric on an independent test set containing a number of datapoints equal to the number of possible quintuple mutations. Different shuffling techniques were applied to different portion of the datasets, which included random or mutant based (Fig. S1). The latter consisted of sorting the dataset (or a subset) accordingly to the number of mutations contained in each variant after randomly shuffling it.

To study the impact of including more information in the training dataset, we generated the LCs (Fig. 2D.1) and the actual vs. predicted scatter plots, also known as calibration plots, at different training

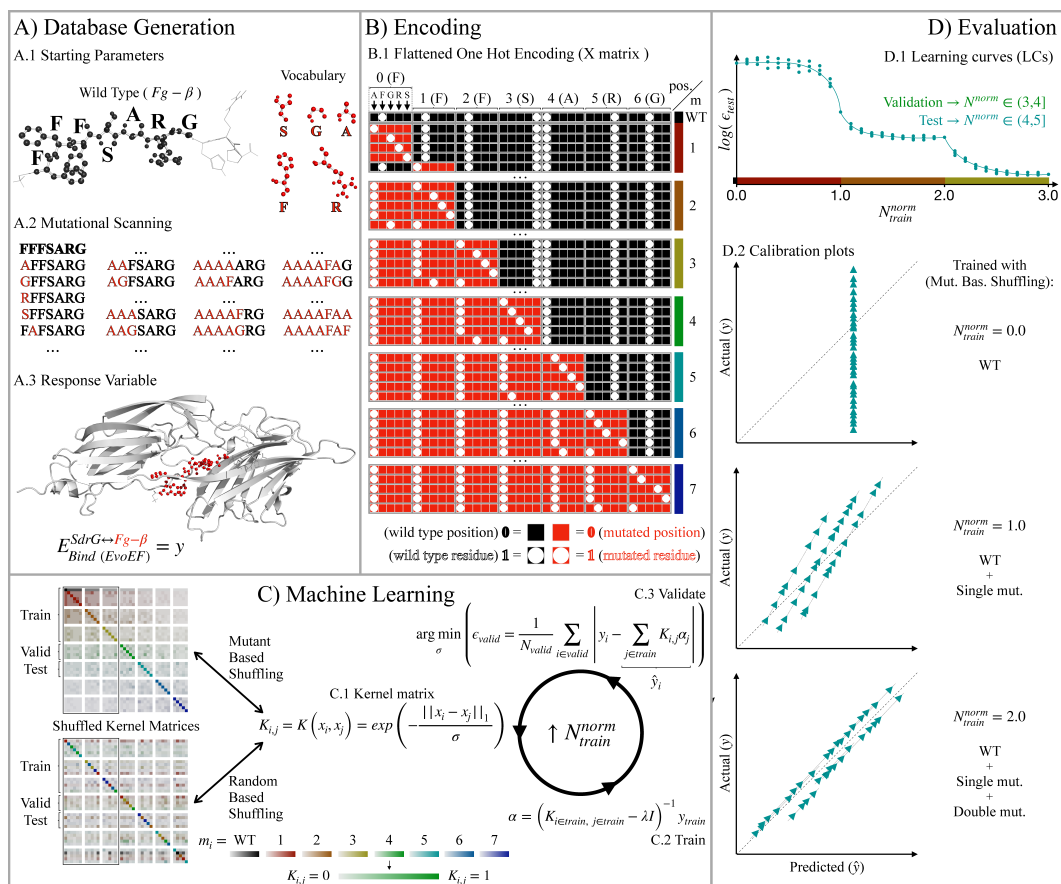


Figure 2: Workflow overview. (A) Database Generation: a table containing all possible mutagenized peptide variants was generated from a starting construct (WT) and a mutational vocabulary. The response variable (binding energy) was computed for each entry. (B) Encoding: the database was converted into a matrix containing numerical values using binary flattened one hot encoding. (C) Machine learning: Laplacian kernel machines were trained using different quantities of data and different shuffling strategies. (D) Evaluation: LCs and calibration plots were used to study the learning process. The amount of information used during training in the scatter plots is reported on the figure.

instances (Fig. 2D.2). In order to account for the non-linearity of the combinatorial nature of our mutagenizable systems (Fig. 1), we developed an alternative way to scale the number of datapoints in the LCs (see Supporting Information, Materials and Methods). The number of datapoints was converted using a formula related to the beta function. To give an example, any number of single mutants (plus WT) can be mapped to a number between zero (one entry) and one (a number equal to all possible single mutants plus the WT). Each unit along the x-axis of the learning curve therefore represented a number of training examples that had saturated mutations of a given order (i.e., 1st order mutations, double mutants, etc.).

## 2.2 Phase-transitioning learning curves (LCs)

The LCs of the biological and chemical systems described above are shown in Fig. 3. We started by analyzing the performance of our kernel machines on two simple functions based on many-body theory (Fig. 3A). We observed two possible regimes arising from feeding the model with mutant-based shuffled data. We called such behaviors “asymptotic” and “saturated” decay. Asymptotic decay was observed for higher order mutations and consisted of a trend similar to the one typically reported, which followed a power law decay tending asymptotically to an offset. In contrast to typical LCs reported in the literature, this behavior was observed strictly within specific regions where a



certain number of mutations were enclosed in the training dataset, but not across the whole LC. In regions not characterized by asymptotic decay, we observed saturated decay. In this scenario, the MAE remained constant in the initial phase and dropped suddenly at the point where most variants with a specific number of mutations had been included (saturated) in the training dataset. In addition, we found that the regions where saturated decay was observed correlated with the order of the function used to generate the response variables. In the case of a linear function (1-body-term) the saturated decay was limited to the single mutant region (Fig. 3A.1,  $N_{train}^{norm} \in (0, 1]$ ), while with a nonlinear function (second order) two saturation decays were observed (Fig. 3A.2,  $N_{train}^{norm} \in (0, 1]$  and  $N_{train}^{norm} \in (1, 2]$ ).

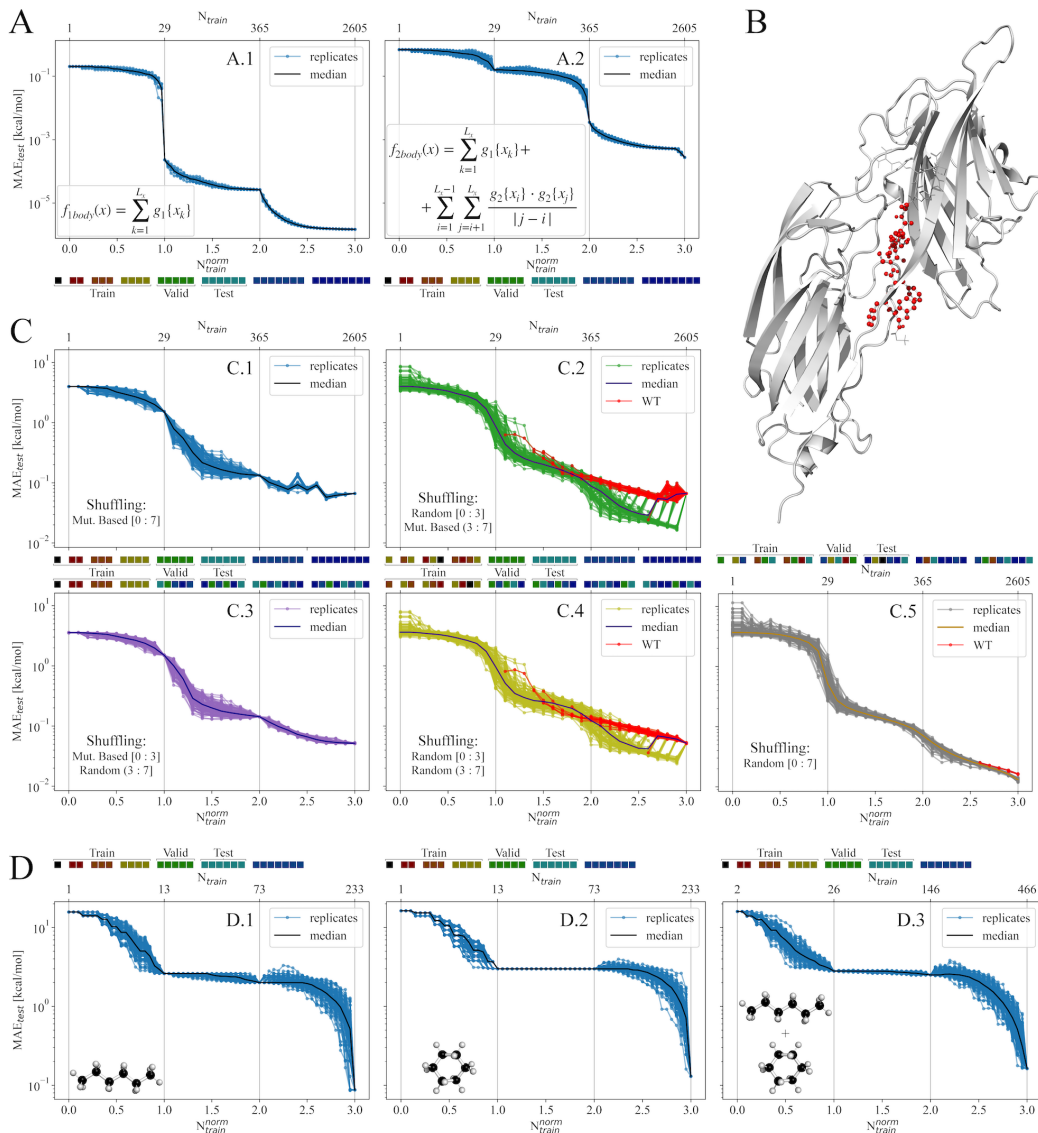


Figure 3: LCs for different discretized spaces and functions. (A) 1-body (left) and 2-body naïve functions. (B) Fg- $\beta$  (red) / *S. epidermidis* adhesin SdrG (greyscale) complex. (C) Binding energy function results using different shuffling. (D) Solvation energies results on different structures (6 heavy atoms linear, cyclic or the combination of both). The shuffling strategies are specified when relevant. If not explicitly specified, mutant-based shuffling is applied to the whole dataset. The presence of WT in the training set is reported in red only if the shuffling strategy did not automatically set it as the first entry.

To determine if this scaling behavior generalized to other functions, we used EvoEF to estimate the affinity (binding energy) between a mutagenized peptide (Fg- $\beta$ ) and a known target protein (SdrG, Fig. 3B). We investigated the influence of the mutant shuffling strategies applied to the dataset on the LCs (Fig. 3C). The training data were shuffled using a mutation-based scheme and the training set was filled in a hierarchical way with up to triple mutants (Fig. 3C.1). The results showed similar behavior to what was previously observed in the 1-body term case (Fig. 3A.1). We observed saturated decay in the single mutant region of the LC ( $N_{train}^{norm} \in (0, 1]$ ), and two asymptotical decays in the double ( $N_{train}^{norm} \in (1, 2]$ ) and triple mutants regions ( $N_{train}^{norm} \in (2, 3]$ ). The latter showed the presence of noise with some spikes in the MAE. This was mitigated by randomly shuffling the variants containing more than 4 mutations, forcing the validation and the test to include all possible mutations above triples (included only in the training set) and making both similarly distributed (Fig. 3C.3). The shuffling strategy of the data which constituted the training set seemed to have the highest impact on the LCs. In fact, if the hierarchical order of the mutations was not maintained in the training set, a new behavior arose. This result was independent from the methodologies employed, irrespective of whether the dataset was randomly shuffled (Fig. 3C.5), the higher order mutations were mutant based shuffled (Fig. 3C.2) or separately randomly shuffled from the lower order mutations (Fig. 3C.4). In such cases, the LCs did not present discontinuities as before but showed acceleration and deceleration. This was also confirmed when we extended the vocabulary of possible mutations (Fig. S2) and when we further restricted the mutagenizable positions (Fig. S3). The presence or absence of the WT (parent) sequence in the training set also strongly affected the path of the corresponding LCs (see below).

In order to extend our findings to a different type discrete combinatorial space, we applied the same methodology to a linear molecular graph (hexane, Fig. 3D.1) and to a cyclic molecule (cyclohexane, Fig. 3D.2). In these scenarios, we observed only saturated decay behavior, independently from the mutations contained in the training set. Furthermore, upon integrating the two molecular datasets, we observed results that were strikingly akin to those previously obtained.

Finally, we studied the impact of the mathematical encoding of our systems. In the peptide scenarios (Fig. S4 and Fig. S5), we utilized a normalized, PCA-reduced version of the AA index database [36] (Tab. S4), and a binned z-score [74] (Tab. S3). The outcomes were congruent with prior observations, reinforcing the initial findings. In the organic small molecule cases, a different outcome was observed when Coulomb matrix encoding [60] was employed (Fig. S6). In such a case, the LCs presented several asymptotic decays, showing that not only the (non-)linearity of the predicted fitness contributes to the LCs behavior, but also the encoding employed. Moreover, when the entire chemical dataset was randomly shuffled, neither acceleration nor deceleration was observed. This phenomenon warrants additional investigation in future studies.

### 2.3 Learning and predicting peptide fitness with variable amounts of training data

For the case study in learning EvoEF binding energy of the Fg- $\beta$  peptide, we next generated calibration plots (Fig. 4A), which consisted of plotting the EvoEF binding fitness values against the results predicted by the ML model. We achieved this by separating the data according to the number of mutations enclosed (Fig. 4A, first row and Fig. S8, column-wise) and by including different information levels in the training set (Fig. 4A, second row and Fig. S8, row-wise). This was done to relate to a realistic scenario where the aim was to explore regions of the search space containing higher number of mutations in comparison to the ones available in the experimental data. In the results presented here, two distinct trends were observed. On one hand, the prediction accuracy of the ML models increased when more information (data) was included in the training set (Fig. 4A, second row), as already observed with the LCs. On the other hand, the model performance scaled inversely with the number of mutations contained in the predicted data (Fig. 4A, first row), highlighting the difficulty of pure ML to extrapolate from the training set.

Another observation was that when the ML model was trained with the WT sequence and all single mutants (Fig. 4A, first row, second column), we noticed a distinct pattern arising from the predictions, where the predicted points formed different parallel clusters (Fig. 4B). These clusters exhibited an angular deviation, relative to the line of "perfect prediction" (Predicted = Actual), indicating a systematic deviation from the ideal alignment. Such deviations seemed to be mitigated by the inclusion of additional information (mutations) in the training set, or by predicting data containing a specific number of mutations, following the same trends observed for the model performance.

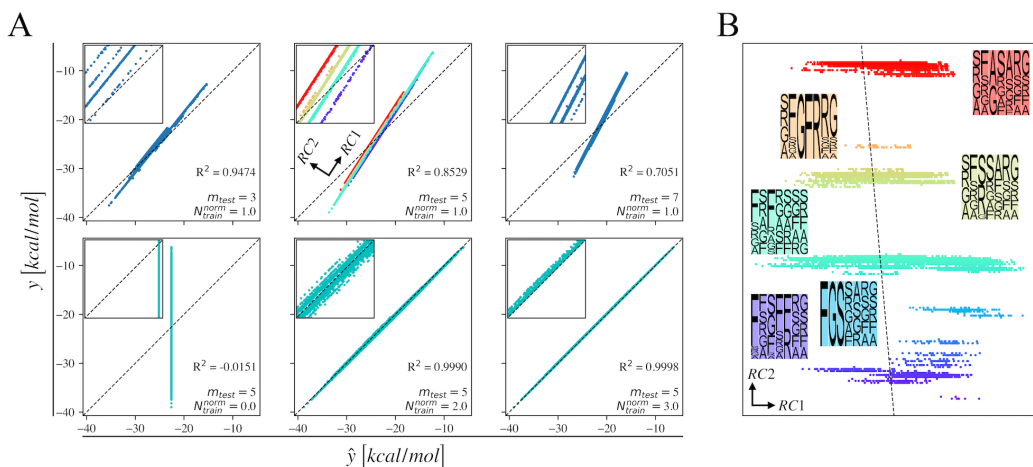


Figure 4: Calibration plots of Fg- $\beta$  / *S. epidermidis* adhesin SdrG complex binding energy function. (A) Scatter plots showing true ( $y$ ) vs. predicted ( $\hat{y}$ ) energies at different numbers of mutations ( $m$ , first row) and training instances ( $N_{training}^{norm}$ , second row). Insets: zoom-in. (B) Rotation of the predictions coming from a ML model trained with the WT and all single mutants and tested on all quintuple mutants (shown in panel A, 1st row, 2nd column). Insets: amino acids frequencies accordingly to their cluster positions.

Moreover, the incorporation of supplementary information in the training set also influenced the clusters dispersion, resulting in a reduced separation among them (Fig. 4A, insets). Upon examining the frequency distribution of mutations within the clusters (Fig. 4B, Fig. S7), we did not identify any specific trends, except for a notable accumulation of phenylalanine (F) at the first position in the lower clusters.

These latest observations led us to further investigate how the predictions were distributed in comparison to the actual values. This was undertaken with an expanded focus, not solely on the learning points where complete sets of mutations were included during training, as previously done, but also at intermediate stages. By adopting this approach, new trends were observed. At first, we concentrated on the phase where the WT and the single mutants were gradually incorporated in the training set (saturated decay, Fig. S9). At the initial stage, where only a limited set of datapoints were included, we observed a superimposing phase (overfitting), in which the test values were simply inferred from the nearest neighbor contained in the training set. This was the natural extension of the scenario where only a single datapoint (the WT) was used for training and a single vertical line was observed in the calibration plots (Fig. 4A, second row, first column). The number of vertical lines identified increased as the training dataset grew, until it reached a point where they could no longer be distinguished from one another. Shortly after, a shift in the learning paradigm appeared to occur, leading to the emergence of different parallel clusters, which no longer resulted vertically aligned plots, but rather tilted plots. Significantly, continuing to add new data points to the training set resulted in the rearranging and merging of such clusters. This behavior persisted until all single mutants, and the WT were incorporated and a minimal count of clusters was achieved. Upon incorporating the double mutants (asymptotical decay, Fig. S10), the clusters once again diverged and became fuzzier in an initial phase, before converging in a different arrangement during the later stage.

A comparable occurrence was observed when the study was extended to many-body response variables, on both linear (Fig. S11, Fig. S12) and non-linear (Fig. S13, Fig. S14) functions. It is important to highlight that in the latter scenario, the clusters that formed did not align linearly but exhibited a non-linear relationship.

## 2.4 The impact of specific sequence examples on learning

Finally, further investigations were conducted to expand upon the preliminary observation presented above regarding the impact of including the WT on the LCs in cases where the training set order was randomized (red paths, Fig. 3C.2, 3C.4 and 3C.5). To achieve this, we extended the LC of

three specific examples by calculating the test MAE on each kernel scale value used during the hyperparameter optimization (Fig. 5). On one hand, when the training set was mutant based shuffled and the remaining mutants were randomly shuffled (Fig. 3C.3), steep valleys arose (Fig. 5A.1 and Fig. 5B.1). The number of such valleys seemed to correlate with the number of mutations included in the mutant based shuffled training dataset (i.e., one for single mutants, two for doubles, etc.). Moreover, the sudden change in the order of magnitude of the optimal hyperparameter, due to a jump from a valley to another one, could partially explain the learning discontinuities observed within this work. On the other hand, when the whole dataset was shuffled (Fig. 3C.5), a trough-like configuration replaced the previous scenario (Fig. 5A.3 and Fig. 5B.3). In this case, the optimal path would follow a gentle, sloping descent down the hills, minimizing steep declines and allowing for a smoother transition to the valley floor, explaining the learning accelerations/decelerations previously observed. The last example showed a situation where the WT sequence was included in the training set in the middle of the LC (Fig. 5A.2 and Fig. 5B.2). We already noted that such incorporation significantly affected the LC path, suddenly increasing the test MAE. Interestingly, the extended LC of this example showed a combination of the two behaviors observed above. In fact, before this critical point, the extended LC presented one single, broad opening. Subsequently, the surface transformed immediately, revealing a scenario where multiple valleys became distinctly evident, similar to what was observed in the mutant based shuffled trained example (Fig. 5A.1 and Fig. 5B.1).

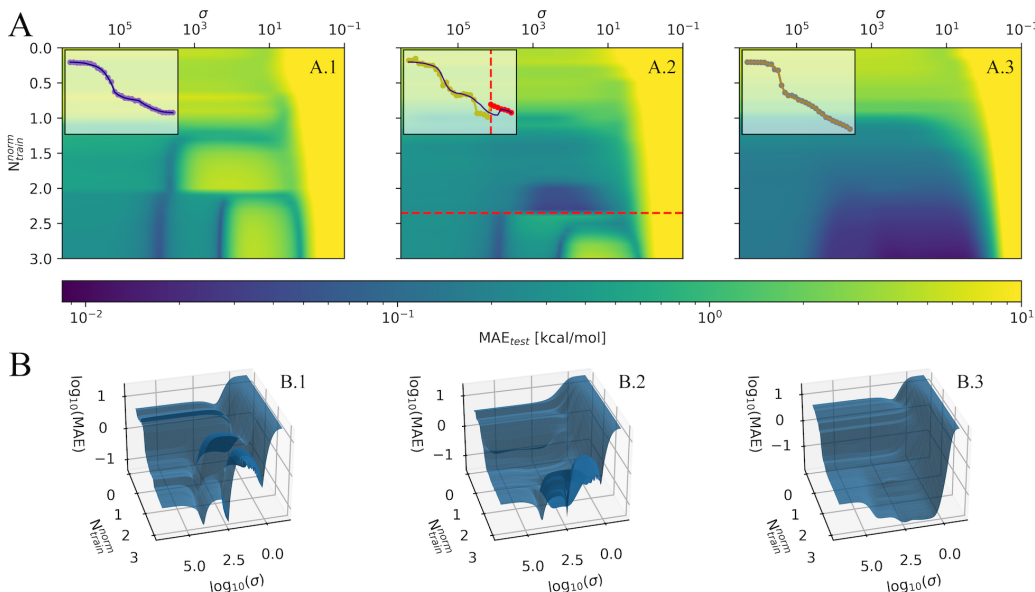


Figure 5: Impact of WT sequence being included in the training data on learning Fg- $\beta$  / SdrG complex binding energy function (EvoEF). (A) Extended LCs (hyperparameter,  $\sigma$ ) of single examples using different shuffling strategies (see Fig. 2). The dashed red lines mark the point at which the WT sequence was included in the training set. Insets: standard LCs of the specific replicates analysed. (B) 3D projection of the plots shown in panel A.

### 3 Conclusion

In this work we studied data-error scaling in machine learning in the context of mutagenisable discrete spaces, in particular a peptide interacting with its target receptor (Fg- $\beta$ :SdrG) and small molecule solvation energies. We leveraged deterministic functions to compute the response variables and generate synthetic datasets. This approach enabled us to focus on a learning process devoid of noise, effectively eliminating variability attributed to experimental errors or non-deterministic simulations.

We presented a novel way to normalize LCs based on mutational saturation of a particular degree, and a new shuffling methodology suitable for any discrete combinatorial input space prone-to-mutations. Our findings indicated that the learning process did not conform to a single power law but might be discontinuous, and categorizable in two distinct regimes (i.e. asymptotical or saturated decay). These

regimes exhibit acceleration and deceleration phases of learning. Such knowledge could be extremely valuable in Design Of Experiments (DOE), as well as in developing theoretical mechanistic models. In the first scenario, given knowledge on the order of the phenomenon involved, a lab scientist could design a variant library to saturate certain numbers of mutations (saturated decay) and to partially cover other ones (asymptotic decay). In the second scenario, analyzing the trajectories of LCs could provide significant insights into the order of the model (i.e., linear or non-linear) that would be appropriate for approximating a physico-chemical phenomena. Based on our results, we showed that learning trajectories can be affected by the shuffling strategy applied to the data, by the encoding strategies employed, and by the natural process leading to the response variable. Furthermore, our analysis demonstrated that test predictions clustered in parallel groups and that the presence of the parent sequence (i.e. WT) from which variants are derived through mutations can dramatically influence the learning process.

Although our findings appear to diverge from previous observations in the domains of theoretical chemistry and physics, this discrepancy may be attributed to the nature of datasets commonly utilized within these fields. Chemistry, as a discipline, focuses predominantly on the de novo design of molecules, prioritizing alterations in molecular graphs over introducing point mutations on existing structures. This approach contrasts with the methodologies typically applied to generate biological DMS data. In fact, most of the potential molecular variants would be highly unstable, which diminishes their practical applicability and, consequently, the incentive to incorporate them into simulations for data generation. Despite this, our results hold value for researchers in molecular disciplines where mutations are feasible. For instance, they could inform studies investigating the effects of varying functional groups at specific positions within a molecule.

Given the complexity of understanding the data-error scalability in the context of discrete input spaces prone-to-mutations, this study focused on noise-free labelled data on point mutated molecular and peptide graphs. Future studies could extend our work by including real or simulated uncertainty in the response variable(s), integrating insertion-deletions (indels) and/or validating our observations on additional mutagenizable spaces. Our findings on data-error scalability could impact the way experimental and simulation campaigns are conducted for mutational data, lowering both the time and the costs of potentially any field where discrete combinatorial inputs prone-to-mutations play a role. This could be achieved directly, by decreasing the necessary runs to produce the data, or indirectly, by focusing the machine learning training on the most information-rich variants. Furthermore, our findings have the potential to broaden the statistical learning theory, contributing to the understanding of how machines learn from specific discrete data.

## Acknowledgments and Disclosure of Funding

This work was supported by the University of Basel, the Swiss Federal Institute of Technology in Zürich (ETH Zürich) and the Swiss Nanoscience Institute (SNI, project P1802). The authors declare that some text was edited using ChatGPT (<https://chat.openai.com>). The editing focused solely on rearranging, enhancing, or correcting the syntax of existing sentences without creating new content. Some of the calculations were performed at sciCORE scientific computing center at the University of Basel (<https://scicore.unibas.ch>). 3D molecular structures were generated and processed with Leruli [21] and PyMOL [63]. QMLCode [16] was utilized for some computations. The authors would like to thank Dr. Dominik Lemm and Dr. Stefan Heinen for the insightful discussions in the preliminary phase of this project.

## References

- [1] Note sur une méthode de résolution des équations normales provenant de l'application de la méthode des moindres carrés a un système d'équations linéaires en nombre inférieur a celui des inconnues. – application de la méthode a la résolution d'un système defini d'équations linéaires. *Bulletin géodésique*, 2(1):67–77, 1924. ISSN 1432-1394. URL <https://doi.org/10.1007/BF03031308>.
- [2] Michael H. Abraham. Scales of solute hydrogen-bonding: their construction and application to physicochemical and biochemical processes. *Chem. Soc. Rev.*, 22(2):73–83, 1993. ISSN 0306-0012. URL <http://dx.doi.org/10.1039/CS9932200073>.

- [3] Ethan C. Alley, Grigory Khimulya, Surojit Biswas, Mohammed AlQuraishi, and George M. Church. Unified rational protein engineering with sequence-based deep representation learning. *Nature Methods*, 16(12):1315–1322, December 2019. ISSN 1548-7105. URL <https://doi.org/10.1038/s41592-019-0598-1>.
- [4] Shun-ichi Amari, Naotake Fujita, and Shigeru Shinomoto. Four types of learning curves. *Neural Comput*, 4(4):605–618, July 1992. ISSN 0899-7667. URL <https://doi.org/10.1162/neco.1992.4.4.605>.
- [5] Ivan Anishchenko, Samuel J. Pellock, Tamuka M. Chidyausiku, Theresa A. Ramelot, Sergey Ovchinnikov, Jingzhou Hao, Khushboo Bafna, Christoffer Norn, Alex Kang, Asim K. Bera, Frank DiMaio, Lauren Carter, Cameron M. Chow, Gaetano T. Montelione, and David Baker. De novo protein design by deep network hallucination. *Nature*, 600(7889):547–552, 2021. ISSN 1476-4687. URL <https://doi.org/10.1038/s41586-021-04184-w>.
- [6] Minkyung Baek and David Baker. Deep learning and protein structure modeling. *Nature Methods*, 19(1):13–14, 2022. ISSN 1548-7105. URL <https://doi.org/10.1038/s41592-021-01360-8>.
- [7] Yasaman Bahri, Ethan Dyer, Jared Kaplan, Jaehoon Lee, and Utkarsh Sharma. Explaining neural scaling laws, 2024.
- [8] Mikhail Belkin, Daniel Hsu, Siyuan Ma, and Soumik Mandal. Reconciling modern machine-learning practice and the classical bias-variance trade-off. *Proceedings of the National Academy of Sciences*, 116(32):15849–15854, August 2019. doi: 10.1073/pnas.1903070116. URL <https://doi.org/10.1073/pnas.1903070116>.
- [9] Ian H. Bell, Jorrit Wronski, Sylvain Quoilin, and Vincent Lemort. Pure and pseudo-pure fluid thermophysical property evaluation and the open-source thermophysical property library coolprop. *Ind. Eng. Chem. Res.*, 53(6):2498–2508, February 2014. ISSN 0888-5885. doi: 10.1021/ie4033999. URL <https://doi.org/10.1021/ie4033999>.
- [10] James Betker, Gabriel Goh, Li Jing, Tim Brooks, Jianfeng Wang, Linjie Li, Long Ouyang, Juntang Zhuang, Joyce Lee, Yufei Guo, et al. Improving image generation with better captions. *Computer Science*. <https://cdn.openai.com/papers/dall-e-3.pdf>, 2023.
- [11] Gwen R. Buel and Kylie J. Walters. Can alphafold2 predict the impact of missense mutations on structure? *Nature Structural & Molecular Biology*, 29(1):1–2, 2022. ISSN 1545-9985. URL <https://doi.org/10.1038/s41594-021-00714-2>.
- [12] Marshall Case, Matthew Smith, Jordan Vinh, and Greg Thurber. Machine learning to predict continuous protein properties from binary cell sorting data and map unseen sequence space. *Proceedings of the National Academy of Sciences*, 121(11):e2311726121, March 2024. doi: 10.1073/pnas.2311726121. URL <https://doi.org/10.1073/pnas.2311726121>.
- [13] Lin Chen, Zehong Zhang, Zhenghao Li, Rui Li, Ruifeng Huo, Lifan Chen, Dingyan Wang, Xiaomin Luo, Kaixian Chen, Cansong Liao, and Mingyue Zheng. Learning protein fitness landscapes with deep mutational scanning data from multiple sources. *Cell Systems*, 14(8):706–721.e5, 2023. ISSN 2405-4712. URL <https://www.sciencedirect.com/science/article/pii/S2405471223002107>.
- [14] Yongcan Chen, Ruyun Hu, Keyi Li, Yating Zhang, Lihao Fu, Jianzhi Zhang, and Tong Si. Deep mutational scanning of an oxygen-independent fluorescent protein creilov for comprehensive profiling of mutational and epistatic effects. *ACS Synth. Biol.*, April 2023. doi: 10.1021/acssynbio.2c00662. URL <https://doi.org/10.1021/acssynbio.2c00662>.
- [15] Jun Cheng, Guido Novati, Joshua Pan, Clare Bycroft, Akvilė Žemgulytė, Taylor Applebaum, Alexander Pritzel, Lai Hong Wong, Michal Zielinski, Tobias Sargeant, Rosalia G. Schneider, Andrew W. Senior, John Jumper, Demis Hassabis, Pushmeet Kohli, and Žiga Avsec. Accurate proteome-wide missense variant effect prediction with alphamissense. *Science*, 381(6664):eadg7492, March 2024. doi: 10.1126/science.adg7492. URL <https://doi.org/10.1126/science.adg7492>.

- [16] AS Christensen, FA Faber, B Huang, LA Bratholm, A Tkatchenko, KR Muller, and OA von Lilienfeld. Qml: A python toolkit for quantum machine learning. URL <https://github.com/qmlcode/qml>, 2017.
- [17] Yunsie Chung, Ryan J. Gillis, and William H. Green. Temperature-dependent vapor-liquid equilibria and solvation free energy estimation from minimal data. *AIChE J*, 66(6):e16976, June 2020. ISSN 0001-1541. URL <https://doi.org/10.1002/aic.16976>.
- [18] Corinna Cortes, L. D. Jackel, Sara Solla, Vladimir Vapnik, and John Denker. Learning curves: Asymptotic values and rate of convergence. In J. Cowan, G. Tesauro, and J. Alspector, editors, *Advances in Neural Information Processing Systems*, volume 6. Morgan-Kaufmann, 1994. URL <https://proceedings.neurips.cc/paper/1993/file/1aa48fc4880bb0c9b8a3bf979d3b917e-Paper.pdf>.
- [19] Volker L. Deringer, Albert P. Bartók, Noam Bernstein, David M. Wilkins, Michele Ceriotti, and Gábor Csányi. Gaussian process regression for materials and molecules. *Chem. Rev.*, 121(16):10073–10141, August 2021. ISSN 0009-2665. doi: 10.1021/acs.chemrev.1c00022. URL <https://doi.org/10.1021/acs.chemrev.1c00022>.
- [20] Jacob Devlin, Ming-Wei Chang, Kenton Lee, and Kristina Toutanova. Bert: Pre-training of deep bidirectional transformers for language understanding, 2019.
- [21] Lemm Dominik, Guido F. von Rudorff, and Anatole O. von Lilienfeld. Leruli.com, online molecular property predictions in real time and for free. [www.leruli.com](http://www.leruli.com), 2021.
- [22] A. Engel and C. Van den Broeck. *Statistical Mechanics of Learning*. Cambridge University Press, Cambridge, 2001. doi: 10.1017/cbo9781139164542. URL <https://www.cambridge.org/core/books/statistical-mechanics-of-learning/D10C20B9997048D27EC08348EE851922>.
- [23] Richard Evans, Michael O’Neill, Alexander Pritzel, Natasha Antropova, Andrew Senior, Tim Green, Augustin Židek, Russ Bates, Sam Blackwell, Jason Yim, Olaf Ronneberger, Sebastian Bodenstein, Michal Zielinski, Alex Bridgland, Anna Potapenko, Andrew Cowie, Kathryn Tunyasuvunakool, Rishub Jain, Ellen Clancy, Pushmeet Kohli, John Jumper, and Demis Hassabis. Protein complex prediction with alphafold-multimer. *bioRxiv*, page 2021.10.04.463034, January 2021. URL <http://biorxiv.org/content/early/2021/10/04/2021.10.04.463034.abstract>.
- [24] Matthew S. Faber and Timothy A. Whitehead. Data-driven engineering of protein therapeutics. *Current Opinion in Biotechnology*, 60:104–110, December 2019. ISSN 0958-1669. URL <http://www.sciencedirect.com/science/article/pii/S0958166918301587>.
- [25] Chase R. Freschlin, Sarah A. Fahlberg, and Philip A. Romero. Machine learning to navigate fitness landscapes for protein engineering. *Current Opinion in Biotechnology*, 75:102713, 2022. ISSN 0958-1669. URL <https://www.sciencedirect.com/science/article/pii/S0958166922000465>.
- [26] Nathan C. Frey, Ryan Soklaski, Simon Axelrod, Siddharth Samsi, Rafael Gómez-Bombarelli, Connor W. Coley, and Vijay Gadepally. Neural scaling of deep chemical models. *Nature Machine Intelligence*, 5(11):1297–1305, 2023. ISSN 2522-5839. URL <https://doi.org/10.1038/s42256-023-00740-3>.
- [27] Maximilian Gantz, Simon Valentin Mathis, Friederike Nintzel, Pietro Lio, and Florian Hollfelder. On synergy between ultrahigh throughput screening and machine learning in biocatalyst engineering. *Faraday Discuss.*, pages –, 2024. doi: 10.1039/D4FD00065J. URL <http://dx.doi.org/10.1039/D4FD00065J>.
- [28] Jonathan C. Greenhalgh, Sarah A. Fahlberg, Brian F. Pflieger, and Philip A. Romero. Machine learning-guided acyl-acyl reductase engineering for improved in vivo fatty alcohol production. *Nature Communications*, 12(1):5825, 2021. ISSN 2041-1723. URL <https://doi.org/10.1038/s41467-021-25831-w>.

- [29] Ryan-Rhys Griffiths, Leo Klarner, Henry Moss, Aditya Ravuri, Sang Truong, Yuanqi Du, Samuel Stanton, Gary Tom, Bojana Rankovic, Arian Jamasb, Aryan Deshwal, Julius Schwartz, Austin Tripp, Gregory Kell, Simon Frieder, Anthony Bourached, Alex Chan, Jacob Moss, Chengzhi Guo, Johannes Peter Dürholt, Saudamini Chaurasia, Ji Won Park, Felix Strieth-Kalthoff, Alpha Lee, Bingqing Cheng, Alan Aspuru-Guzik, Philippe Schwaller, and Jian Tang. Gauche: A library for gaussian processes in chemistry. In A. Oh, T. Naumann, A. Globerson, K. Saenko, M. Hardt, and S. Levine, editors, *Advances in Neural Information Processing Systems*, volume 36, pages 76923–76946. Curran Associates, Inc., 2023. URL [https://proceedings.neurips.cc/paper\\_files/paper/2023/file/f2b1b2e974fa5ea622dd87f22815f423-Paper-Conference.pdf](https://proceedings.neurips.cc/paper_files/paper/2023/file/f2b1b2e974fa5ea622dd87f22815f423-Paper-Conference.pdf).
- [30] Bing Huang, Guido Falk von Rudorff, and O. Anatole von Lilienfeld. The central role of density functional theory in the ai age. *Science*, 381(6654):170–175, July 2023. doi: 10.1126/science.abn3445. URL <https://doi.org/10.1126/science.abn3445>.
- [31] Xiaoqiang Huang, Robin Pearce, and Yang Zhang. Evoef2: accurate and fast energy function for computational protein design. *Bioinformatics (Oxford, England)*, 36(31588495):1135–1142, February 2020. ISSN 1367-4803. URL <https://www.ncbi.nlm.nih.gov/pmc/articles/PMC7144094/>.
- [32] Albert Q. Jiang, Alexandre Sablayrolles, Arthur Mensch, Chris Bamford, Devendra Singh Chaplot, Diego de las Casas, Florian Bressand, Gianna Lengyel, Guillaume Lample, Lucile Saulnier, L lio Renard Lavaud, Marie-Anne Lachaux, Pierre Stock, Teven Le Scao, Thibaut Lavril, Thomas Wang, Timoth e Lacroix, and William El Sayed. Mistral 7b, 2023.
- [33] Allison Judge, Banumathi Sankaran, Liya Hu, Murugesan Palaniappan, Andr  Birgy, B. V. Venkataram Prasad, and Timothy Palzkill. Network of epistatic interactions in an enzyme active site revealed by large-scale deep mutational scanning. *Proceedings of the National Academy of Sciences*, 121(12):e2313513121, March 2024. doi: 10.1073/pnas.2313513121. URL <https://doi.org/10.1073/pnas.2313513121>.
- [34] John Jumper, Richard Evans, Alexander Pritzel, Tim Green, Michael Figurnov, Olaf Ronneberger, Kathryn Tunyasuvunakool, Russ Bates, Augustin  idek, Anna Potapenko, Alex Bridgland, Clemens Meyer, Simon A. A. Kohl, Andrew J. Ballard, Andrew Cowie, Bernardino Romera-Paredes, Stanislav Nikolov, Rishub Jain, Jonas Adler, Trevor Back, Stig Petersen, David Reiman, Ellen Clancy, Michal Zielinski, Martin Steinegger, Michalina Pacholska, Tamas Berghammer, Sebastian Bodenstern, David Silver, Oriol Vinyals, Andrew W. Senior, Koray Kavukcuoglu, Pushmeet Kohli, and Demis Hassabis. Highly accurate protein structure prediction with alphafold. *Nature*, 596(7873):583–589, 2021. ISSN 1476-4687. URL <https://doi.org/10.1038/s41586-021-03819-2>.
- [35] Jared Kaplan, Sam McCandlish, Tom Henighan, Tom B. Brown, Benjamin Chess, Rewon Child, Scott Gray, Alec Radford, Jeffrey Wu, and Dario Amodei. Scaling laws for neural language models, 2020.
- [36] Shuichi Kawashima, Piotr Pokarowski, Maria Pokarowska, Andrzej Kolinski, Toshiaki Katayama, and Minoru Kanehisa. AAindex: amino acid index database, progress report 2008. *Nucleic Acids Res.*, 36(Database issue):D202–5, January 2008.
- [37] Hyeonsu Kim, Jeheon Woo, SEONGHWAN KIM, Seokhyun Moon, Jun Hyeong Kim, and Woo Youn Kim. Geotmi: Predicting quantum chemical property with easy-to-obtain geometry via positional denoising. In A. Oh, T. Naumann, A. Globerson, K. Saenko, M. Hardt, and S. Levine, editors, *Advances in Neural Information Processing Systems*, volume 36, pages 46027–46040. Curran Associates, Inc., 2023. URL [https://proceedings.neurips.cc/paper\\_files/paper/2023/file/903c5eb12f2389c4847574df90503d63-Paper-Conference.pdf](https://proceedings.neurips.cc/paper_files/paper/2023/file/903c5eb12f2389c4847574df90503d63-Paper-Conference.pdf).
- [38] Dominik Lemm, Guido Falk von Rudorff, and O. Anatole von Lilienfeld. Machine learning based energy-free structure predictions of molecules, transition states, and solids. *Nature Communications*, 12(1):4468, 2021. ISSN 2041-1723. URL <https://doi.org/10.1038/s41467-021-24525-7>.



- [39] Marc F. Lensink, Guillaume Brysbaert, Nessim Raouraoua, Paul A. Bates, Marco Giulini, Rodrigo V. Honorato, Charlotte van Noort, Joao M. C. Teixeira, Alexandre M. J. J. Bonvin, Ren Kong, Hang Shi, Xufeng Lu, Shan Chang, Jian Liu, Zhiye Guo, Xiao Chen, Alex Morehead, Raj S. Roy, Tianqi Wu, Nabin Giri, Farhan Qadir, Chen Chen, Jianlin Cheng, Carlos A. Del Carpio, Eichiro Ichiishi, Luis A. Rodriguez-Lumbresas, Juan Fernandez-Recio, Ameya Harmalkar, Lee-Shin Chu, Sam Canner, Rituparna Smanta, Jeffrey J. Gray, Hao Li, Peicong Lin, Jiahua He, Huanyu Tao, Sheng-You Huang, Jorge Roel-Touris, Brian Jimenez-Garcia, Charles W. Christoffer, Anika J. Jain, Yuki Kagaya, Harini Kannan, Tsukasa Nakamura, Genki Terashi, Jacob C. Verburgt, Yuanyuan Zhang, Zicong Zhang, Hayato Fujuta, Masakazu Sekijima, Daisuke Kihara, Omeir Khan, Sergei Kotelnikov, Usman Ghani, Dzmitry Padhorny, Dmitri Beglov, Sandor Vajda, Dima Kozakov, Surendra S. Negi, Tiziana Ricciardelli, Didier Barradas-Bautista, Zhen Cao, Mohit Chawla, Luigi Cavallo, Romina Oliva, Rui Yin, Melyssa Cheung, Johnathan D. Guest, Jessica Lee, Brian G. Pierce, Ben Shor, Tomer Cohen, Matan Halfon, Dina Schneidman-Duhovny, Shaowen Zhu, Rujie Yin, Yuanfei Sun, Yang Shen, Martyna Maszota-Zieleniak, Krzysztof K. Bojarski, Emilia A. Lubecka, Mateusz Marcisz, Annemarie Danielsson, Lukasz Dziadek, Margrethe Gaardlos, Artur Gieldon, Adam Liwo, Sergey A. Samsonov, Rafal Slusarz, Karolina Zieba, Adam K. Sieradzan, Cezary Czaplewski, Shinpei Kobayashi, Yuta Miyakawa, Yasuomi Kiyota, Mayuko Takeda-Shitaka, Kliment Olechnovic, Lukas Valancauskas, Justas Dapkunas, Ceslovas Venclovas, Bjorn Wallner, Lin Yang, Chengyu Hou, Xiaodong He, Shuai Guo, Shenda Jiang, Xiaoliang Ma, Rui Duan, Liming Qui, Xianjin Xu, Xiaoqin Zou, Sameer Velankar, and Shoshana J. Wodak. Impact of alphafold on structure prediction of protein complexes: The casp15-capri experiment. *Proteins*, 91(12):1658–1683, December 2023. ISSN 0887-3585. URL <https://doi.org/10.1002/prot.26609>.
- [40] Tianyu Liu, Yuge Wang, Rex Ying, and Hongyu Zhao. Muse-gnn: Learning unified gene representation from multimodal biological graph data. In A. Oh, T. Nauemann, A. Globerson, K. Saenko, M. Hardt, and S. Levine, editors, *Advances in Neural Information Processing Systems*, volume 36, pages 24661–24677. Curran Associates, Inc., 2023. URL [https://proceedings.neurips.cc/paper\\_files/paper/2023/file/4db8a681ae1e58376dc6227978829063-Paper-Conference.pdf](https://proceedings.neurips.cc/paper_files/paper/2023/file/4db8a681ae1e58376dc6227978829063-Paper-Conference.pdf).
- [41] Baek Minkyung, DiMaio Frank, Anishchenko Ivan, Dauparas Justas, Ovchinnikov Sergey, Lee Gyu Rie, Wang Jue, Cong Qian, N. Kinch Lisa, Schaeffer R. Dustin, Millán Claudia, Park Hahnbeom, Adams Carson, R. Glassman Caleb, DeGiovanni Andy, H. Pereira Jose, V. Rodrigues Andria, van Dijk Alberdina A., C. Ebrecht Ana, J. Opperman Diederik, Sagmeister Theo, Buhlheller Christoph, Pavkov-Keller Tea, K. Rathinaswamy Manoj, Dalwadi Udit, K. Yip Calvin, E. Burke John, Garcia K. Christopher, V. Grishin Nick, D. Adams Paul, J. Read Randy, and Baker David. Accurate prediction of protein structures and interactions using a three-track neural network. *Science*, 373(6557):871–876, August 2021. doi: 10.1126/science.abj8754. URL <https://doi.org/10.1126/science.abj8754>.
- [42] Christina Mintz, Michael Clark, William E. Acree, and Michael H. Abraham. Enthalpy of solvation correlations for gaseous solutes dissolved in water and in 1-octanol based on the abraham model. *J. Chem. Inf. Model.*, 47(1):115–121, January 2007. ISSN 1549-9596. doi: 10.1021/ci600402n. URL <https://doi.org/10.1021/ci600402n>.
- [43] Grégoire Montavon, Katja Hansen, Siamac Fazli, Matthias Rupp, Franziska Biegler, Andreas Ziehe, Alexandre Tkatchenko, Anatole Lilienfeld, and Klaus-Robert Müller. Learning invariant representations of molecules for atomization energy prediction. *Advances in neural information processing systems*, 25, 2012.
- [44] K.-R. Müller, M. Finke, N. Murata, K. Schulten, and S. Amari. A numerical study on learning curves in stochastic multilayer feedforward networks. *Neural Comput.*, 8(5):1085–1106, July 1996. ISSN 0899-7667. URL <https://doi.org/10.1162/neco.1996.8.5.1085>.
- [45] Pascal Notin, Nathan Rollins, Yarin Gal, Chris Sander, and Debora Marks. Machine learning for functional protein design. *Nature Biotechnology*, 42(2):216–228, 2024. ISSN 1546-1696. URL <https://doi.org/10.1038/s41587-024-02127-0>.
- [46] OpenAI. Gpt-4 technical report, 2023.

- [47] Manfred Opper. Statistical mechanics of learning: Generalization. *The handbook of brain theory and neural networks*, pages 922–925, 1995.
- [48] Carlos Outeiral and Charlotte M. Deane. Codon language embeddings provide strong signals for use in protein engineering. *Nature Machine Intelligence*, 6(2):170–179, 2024. ISSN 2522-5839. URL <https://doi.org/10.1038/s42256-024-00791-0>.
- [49] Marina A. Pak, Karina A. Markhieva, Mariia S. Novikova, Dmitry S. Petrov, Ilya S. Vorobyev, Ekaterina S. Maksimova, Fyodor A. Kondrashov, and Dmitry N. Ivankov. Using alphafold to predict the impact of single mutations on protein stability and function. *PLOS ONE*, 18(3):e0282689, March 2023. doi: 10.1371/journal.pone.0282689. URL <https://doi.org/10.1371/journal.pone.0282689>.
- [50] Robin Pearce, Xiaoqiang Huang, Dani Setiawan, and Yang Zhang. Evodesign: Designing protein-protein binding interactions using evolutionary interface profiles in conjunction with an optimized physical energy function. *Journal of molecular biology*, 431(30851277):2467–2476, June 2019. ISSN 0022-2836. URL <https://www.ncbi.nlm.nih.gov/pmc/articles/PMC6589126/>.
- [51] James A. Platts, Darko Butina, Michael H. Abraham, and Anne Hersey. Estimation of molecular linear free energy relation descriptors using a group contribution approach. *J. Chem. Inf. Comput. Sci.*, 39(5):835–845, September 1999. ISSN 0095-2338. doi: 10.1021/ci980339t. URL <https://doi.org/10.1021/ci980339t>.
- [52] Karthe Ponnuraj, M. Gabriela Bowden, Stacey Davis, S. Gurusiddappa, Dwight Moore, Damon Choe, Yi Xu, Magnus Hook, and Sthanam V. L. Narayana. A “dock, lock, and latch” structural model for a staphylococcal adhesin binding to fibrinogen. *Cell*, 115(2):217–228, 2003. ISSN 0092-8674. URL <https://www.sciencedirect.com/science/article/pii/S0092867403008092>.
- [53] Aditya Ramesh, Mikhail Pavlov, Gabriel Goh, Scott Gray, Chelsea Voss, Alec Radford, Mark Chen, and Ilya Sutskever. Zero-shot text-to-image generation, 2021.
- [54] Aditya Ramesh, Prafulla Dhariwal, Alex Nichol, Casey Chu, and Mark Chen. Hierarchical text-conditional image generation with clip latents, 2022. URL <https://arxiv.org/abs/2204.06125>.
- [55] Jacob T. Rapp, Bennett J. Bremer, and Philip A. Romero. Self-driving laboratories to autonomously navigate the protein fitness landscape. *Nature Chemical Engineering*, 1(1):97–107, 2024. ISSN 2948-1198. URL <https://doi.org/10.1038/s44286-023-00002-4>.
- [56] Carl Edward Rasmussen and Christopher K. I. Williams. *Gaussian Processes for Machine Learning*. The MIT Press, 2006.
- [57] Robin Rombach, Andreas Blattmann, Dominik Lorenz, Patrick Esser, and Björn Ommer. High-resolution image synthesis with latent diffusion models. In *Proceedings of the IEEE/CVF conference on computer vision and pattern recognition*, pages 10684–10695, 2022.
- [58] Philip A. Romero and Frances H. Arnold. Exploring protein fitness landscapes by directed evolution. *Nature reviews. Molecular cell biology*, 10:866–76, Dec 2009.
- [59] Philip A. Romero, Tuan M. Tran, and Adam R. Abate. Dissecting enzyme function with microfluidic-based deep mutational scanning. *Proc Natl Acad Sci USA*, 112(23):7159, June 2015. URL <http://www.pnas.org/content/112/23/7159.abstract>.
- [60] Matthias Rupp, Alexandre Tkatchenko, Klaus-Robert Müller, and O. Anatole von Lilienfeld. Fast and accurate modeling of molecular atomization energies with machine learning. *Phys. Rev. Lett.*, 108:058301, Jan 2012. doi: 10.1103/PhysRevLett.108.058301. URL <https://link.aps.org/doi/10.1103/PhysRevLett.108.058301>.
- [61] Lauren M. Sanders, Ryan T. Scott, Jason H. Yang, Amina Ann Qutub, Hector Garcia Martin, Daniel C. Berrios, Jaden J. A. Hastings, Jon Rask, Graham Mackintosh, Adrienne L. Hoarfrost, Stuart Chalk, John Kalantari, Kia Khezeli, Erik L. Antonsen, Joel Babdor, Richard Barker,

- Sergio E. Baranzini, Afshin Beheshti, Guillermo M. Delgado-Aparicio, Benjamin S. Glicksberg, Casey S. Greene, Melissa Haendel, Arif A. Hamid, Philip Heller, Daniel Jamieson, Katelyn J. Jarvis, Svetlana V. Komarova, Matthieu Komorowski, Prachi Kothiyal, Ashish Mahabal, Uri Manor, Christopher E. Mason, Mona Matar, George I. Mias, Jack Miller, Jerry G. Myers, Charlotte Nelson, Jonathan Oribello, Seung-min Park, Patricia Parsons-Wingerter, R. K. Prabhu, Robert J. Reynolds, Amanda Saravia-Butler, Suchi Saria, Aenor Sawyer, Nitin Kumar Singh, Michael Snyder, Frank Soboczanski, Karthik Soman, Corey A. Theriot, David Van Valen, Kasthuri Venkateswaran, Liz Warren, Liz Worthey, Marinka Zitnik, and Sylvain V. Costes. Biological research and self-driving labs in deep space supported by artificial intelligence. *Nature Machine Intelligence*, 5(3):208–219, 2023. ISSN 2522-5839. URL <https://doi.org/10.1038/s42256-023-00618-4>.
- [62] Axel Sauer, Dominik Lorenz, Andreas Blattmann, and Robin Rombach. Adversarial diffusion distillation, 2023.
- [63] Schrödinger, LLC. The PyMOL molecular graphics system, version 2.5.2. -, November 2015.
- [64] Andrew W. Senior, Richard Evans, John Jumper, James Kirkpatrick, Laurent Sifre, Tim Green, Chongli Qin, Augustin Židek, Alexander W. R. Nelson, Alex Bridgland, Hugo Penedones, Stig Petersen, Karen Simonyan, Steve Crossan, Pushmeet Kohli, David T. Jones, David Silver, Koray Kavukcuoglu, and Demis Hassabis. Improved protein structure prediction using potentials from deep learning. *Nature*, January 2020. ISSN 1476-4687. URL <https://doi.org/10.1038/s41586-019-1923-7>.
- [65] H. S. Seung, H. Sompolinsky, and N. Tishby. Statistical mechanics of learning from examples. *PRA*, 45(8):6056–6091, April 1992. URL <https://link.aps.org/doi/10.1103/PhysRevA.45.6056>.
- [66] Utkarsh Sharma and Jared Kaplan. Scaling laws from the data manifold dimension. *Journal of Machine Learning Research*, 23(9):1–34, 2022. URL <http://jmlr.org/papers/v23/20-1111.html>.
- [67] H. Sompolinsky, N. Tishby, and H. S. Seung. Learning from examples in large neural networks. *Phys. Rev. Lett.*, 65:1683–1686, Sep 1990. doi: 10.1103/PhysRevLett.65.1683. URL <https://link.aps.org/doi/10.1103/PhysRevLett.65.1683>.
- [68] Ben Sorscher, Robert Geirhos, Shashank Shekhar, Surya Ganguli, and Ari Morcos. Beyond neural scaling laws: beating power law scaling via data pruning. In S. Koyejo, S. Mohamed, A. Agarwal, D. Belgrave, K. Cho, and A. Oh, editors, *Advances in Neural Information Processing Systems*, volume 35, pages 19523–19536. Curran Associates, Inc., 2022. URL [https://proceedings.neurips.cc/paper\\_files/paper/2022/file/7b75da9b61eda40fa35453ee5d077df6-Paper-Conference.pdf](https://proceedings.neurips.cc/paper_files/paper/2022/file/7b75da9b61eda40fa35453ee5d077df6-Paper-Conference.pdf).
- [69] Gemini Team, Rohan Anil, Sebastian Borgeaud, Yonghui Wu, Jean-Baptiste Alayrac, Jiahui Yu, Radu Soricut, Johan Schalkwyk, Andrew M. Dai, Anja Hauth, Katie Millican, David Silver, Slav Petrov, Melvin Johnson, Ioannis Antonoglou, Julian Schrittwieser, Amelia Glaese, Jilin Chen, Emily Pitler, Timothy Lillicrap, Angeliki Lazaridou, Orhan Firat, James Molloy, Michael Isard, Paul R. Barham, Tom Hennigan, Benjamin Lee, Fabio Viola, Malcolm Reynolds, Yuanzhong Xu, Ryan Doherty, Eli Collins, Clemens Meyer, Eliza Rutherford, Erica Moreira, Kareem Ayoub, Megha Goel, George Tucker, Enrique Piqueras, Maxim Krikun, Iain Barr, Nikolay Savinov, Ivo Danihelka, Becca Roelofs, Anaïs White, Anders Andreassen, Tamara von Glehn, Lakshman Yagati, Mehran Kazemi, Lucas Gonzalez, Misha Khalman, Jakub Sygnowski, Alexandre Frechette, Charlotte Smith, Laura Culp, Lev Proleev, Yi Luan, Xi Chen, James Lottes, Nathan Schucher, Federico Lebron, Alban Rustemi, Natalie Clay, Phil Crone, Tomas Kocisky, Jeffrey Zhao, Bartek Perz, Dian Yu, Heidi Howard, Adam Bloniarz, Jack W. Rae, Han Lu, Laurent Sifre, Marcello Maggioni, Fred Alcober, Dan Garrette, Megan Barnes, Shantanu Thakoor, Jacob Austin, Gabriel Barth-Maron, William Wong, Rishabh Joshi, Rahma Chaabouni, Deeni Fatiha, Arun Ahuja, Ruibo Liu, Yunxuan Li, Sarah Cogan, Jeremy Chen, Chao Jia, Chenjie Gu, Qiao Zhang, Jordan Grimstad, Ale Jakse Hartman, Martin Chadwick, Gaurav Singh Tomar, Xavier Garcia, Evan Senter, Emanuel Taropa, Thanumalayan Sankaranarayana Pillai, Jacob Devlin, Michael Laskin, Diego de Las Casas, Dasha Valter, Connie Tao, Lorenzo Blanco,

Adrià Puigdomènech Badia, David Reitter, Mianna Chen, Jenny Brennan, Clara Rivera, Sergey Brin, Shariq Iqbal, Gabriela Surita, Jane Labanowski, Abhi Rao, Stephanie Winkler, Emilio Parisotto, Yiming Gu, Kate Olszewska, Yujing Zhang, Ravi Addanki, Antoine Miech, Annie Louis, Laurent El Shafey, Denis Teplyashin, Geoff Brown, Elliot Catt, Nithya Attaluri, Jan Balaguer, Jackie Xiang, Pidong Wang, Zoe Ashwood, Anton Briukhov, Albert Webson, Sanjay Ganapathy, Smit Sanghavi, Ajay Kannan, Ming-Wei Chang, Axel Stjerngren, Josip Djolonga, Yuting Sun, Ankur Bapna, Matthew Aitchison, Pedram Pejman, Henryk Michalewski, Tianhe Yu, Cindy Wang, Juliette Love, Junwhan Ahn, Dawn Bloxwich, Kehang Han, Peter Humphreys, Thibault Sellam, James Bradbury, Varun Godbole, Sina Samangooei, Bogdan Damoc, Alex Kaskasoli, Sébastien M. R. Arnold, Vijay Vasudevan, Shubham Agrawal, Jason Riesa, Dmitry Lepikhin, Richard Tanburn, Srivatsan Srinivasan, Hyeontaek Lim, Sarah Hodgkinson, Pranav Shyam, Johan Ferret, Steven Hand, Ankush Garg, Tom Le Paine, Jian Li, Yujia Li, Minh Giang, Alexander Neitz, Zaheer Abbas, Sarah York, Machel Reid, Elizabeth Cole, Aakanksha Chowdhery, Dipanjan Das, Dominika Rogozińska, Vitaly Nikolaev, Pablo Sprechmann, Zachary Nado, Lukas Zilka, Flavien Prost, Luheng He, Marianne Monteiro, Gaurav Mishra, Chris Welty, Josh Newlan, Dawei Jia, Miltiadis Allamanis, Clara Huiyi Hu, Raoul de Liedekerke, Justin Gilmer, Carl Saroufim, Shruti Rijhwani, Shaobo Hou, Disha Shrivastava, Anirudh Baddepudi, Alex Goldin, Adnan Ozturel, Albin Cassirer, Yunhan Xu, Daniel Sohn, Devendra Sachan, Reinald Kim Amplayo, Craig Swanson, Dessie Petrova, Shashi Narayan, Arthur Guez, Siddhartha Brahma, Jessica Landon, Miteyan Patel, Ruizhe Zhao, Kevin Villela, Luyu Wang, Wenhao Jia, Matthew Rahtz, Mai Giménez, Legg Yeung, Hanzhao Lin, James Keeling, Petko Georgiev, Diana Mincu, Boxi Wu, Salem Haykal, Rachel Saputro, Kiran Vodrahalli, James Qin, Zeynep Cankara, Abhanshu Sharma, Nick Fernando, Will Hawkins, Behnam Neyshabur, Solomon Kim, Adrian Hutter, Priyanka Agrawal, Alex Castro-Ros, George van den Driessche, Tao Wang, Fan Yang, Shuo yin Chang, Paul Komarek, Ross McIlroy, Mario Lučić, Guodong Zhang, Wael Farhan, Michael Sharman, Paul Natsev, Paul Michel, Yong Cheng, Yamini Bansal, Siyuan Qiao, Kris Cao, Siamak Shakeri, Christina Butterfield, Justin Chung, Paul Kishan Rubenstein, Shivani Agrawal, Arthur Mensch, Kedar Soparkar, Karel Lenc, Timothy Chung, Aedan Pope, Loren Maggiore, Jackie Kay, Priya Jhakra, Shibo Wang, Joshua Maynez, Mary Phuong, Taylor Tobin, Andrea Tacchetti, Maja Trebacz, Kevin Robinson, Yash Katariya, Sebastian Riedel, Paige Bailey, Kefan Xiao, Nimesh Ghelani, Lora Aroyo, Ambrose Slone, Neil Houlsby, Xuehan Xiong, Zhen Yang, Elena Gribovskaya, Jonas Adler, Mateo Wirth, Lisa Lee, Music Li, Thais Kagohara, Jay Pavagadhi, Sophie Bridgers, Anna Bortsova, Sanjay Ghemawat, Zafarali Ahmed, Tianqi Liu, Richard Powell, Vijay Bolina, Mariko Iinuma, Polina Zablotskaia, James Besley, Da-Woon Chung, Timothy Dozat, Ramona Comanescu, Xiance Si, Jeremy Greer, Guolong Su, Martin Polacek, Raphaël Lopez Kaufman, Simon Tokumine, Hexiang Hu, Elena Buchatskaya, Yingjie Miao, Mohamed Elhawaty, Aditya Siddhant, Nenad Tomasev, Jinwei Xing, Christina Greer, Helen Miller, Shereen Ashraf, Aurko Roy, Zizhao Zhang, Ada Ma, Angelos Filos, Milos Besta, Rory Blevins, Ted Klimentko, Chih-Kuan Yeh, Soravit Changpinyo, Jiaqi Mu, Oscar Chang, Mantas Pajarskas, Carrie Muir, Vered Cohen, Charline Le Lan, Krishna Haridasan, Amit Marathe, Steven Hansen, Sholto Douglas, Rajkumar Samuel, Mingqiu Wang, Sophia Austin, Chang Lan, Jiepu Jiang, Justin Chiu, Jaime Alonso Lorenzo, Lars Lowe Sjösund, Sébastien Cevey, Zach Gleicher, Thi Avrahami, Anudhyan Boral, Hansa Srinivasan, Vittorio Selo, Rhys May, Konstantinos Aisopos, Léonard Hussenot, Livio Baldini Soares, Kate Baumli, Michael B. Chang, Adrià Recasens, Ben Caine, Alexander Pritzel, Filip Pavetic, Fabio Pardo, Anita Gergely, Justin Frye, Vinay Ramasesh, Dan Horgan, Kartikeya Badola, Nora Kassner, Subhrajit Roy, Ethan Dyer, Víctor Campos, Alex Tomala, Yunhao Tang, Dalia El Badawy, Elspeth White, Basil Mustafa, Oran Lang, Abhishek Jindal, Sharad Vikram, Zhitao Gong, Sergi Caelles, Ross Hemsley, Gregory Thornton, Fangxiaoyu Feng, Wojciech Stokowiec, Ce Zheng, Phoebe Thacker, Çağlar Ünlü, Zhishuai Zhang, Mohammad Saleh, James Svensson, Max Bileschi, Piyush Patil, Ankesh Anand, Roman Ring, Katerina Tsihlias, Arpi Vezer, Marco Selvi, Toby Shevlane, Mikel Rodriguez, Tom Kwiatkowski, Samira Daruki, Keran Rong, Allan Dafoe, Nicholas FitzGerald, Keren Gu-Lemberg, Mina Khan, Lisa Anne Hendricks, Marie Pellat, Vladimir Feinberg, James Cobon-Kerr, Tara Sainath, Maribeth Rauh, Sayed Hadi Hashemi, Richard Ives, Yana Hasson, YaGuang Li, Eric Noland, Yuan Cao, Nathan Byrd, Le Hou, Qingze Wang, Thibault Sottiaux, Michela Paganini, Jean-Baptiste Lespiau, Alexandre Moufarek, Samer Hassan, Kaushik Shivakumar, Joost van Amersfoort, Amol Mandhane, Pratik Joshi, Anirudh Goyal, Matthew Tung, Andrew Brock, Hannah Sheahan, Vedant Misra, Cheng Li, Nemanja Rakićević, Mostafa Dehghani, Fangyu Liu, Sid Mittal, Junhyuk Oh, Seb Noury, Eren

Sezener, Fantine Huot, Matthew Lamm, Nicola De Cao, Charlie Chen, Gamaleldin Elsayed, Ed Chi, Mahdis Mahdieh, Ian Tenney, Nan Hua, Ivan Petrychenko, Patrick Kane, Dylan Scandinaro, Rishub Jain, Jonathan Uesato, Romina Datta, Adam Sadovsky, Oskar Bunyan, Dominik Rabiej, Shimu Wu, John Zhang, Gautam Vasudevan, Edouard Leurent, Mahmoud Alnahlawi, Ionut Georgescu, Nan Wei, Ivy Zheng, Betty Chan, Pam G Rabinovitch, Piotr Stanczyk, Ye Zhang, David Steiner, Subhajit Naskar, Michael Azzam, Matthew Johnson, Adam Paszke, Chung-Cheng Chiu, Jaume Sanchez Elias, Afroz Mohiuddin, Faizan Muhammad, Jin Miao, Andrew Lee, Nino Vieillard, Sahitya Potluri, Jane Park, Elnaz Davoodi, Jiageng Zhang, Jeff Stanway, Drew Garmon, Abhijit Karmarkar, Zhe Dong, Jong Lee, Aviral Kumar, Luwei Zhou, Jonathan Evens, William Isaac, Zhe Chen, Johnson Jia, Anselm Levskaia, Zhenkai Zhu, Chris Gorgolewski, Peter Grabowski, Yu Mao, Alberto Magni, Kaisheng Yao, Javier Snaider, Norman Casagrande, Paul Suganthan, Evan Palmer, Geoffrey Irving, Edward Loper, Manaal Faruqui, Isha Arkatkar, Nanxin Chen, Izhak Shafran, Michael Fink, Alfonso Castaño, Irene Giannoumis, Wooyeol Kim, Mikołaj Rybiński, Ashwin Sreevatsa, Jennifer Prendki, David Soergel, Adrian Goedeckemeyer, Willi Gierke, Mohsen Jafari, Meenu Gaba, Jeremy Wiesner, Diana Gage Wright, Yawen Wei, Harsha Vashisht, Yana Kulizhskaya, Jay Hoover, Maigo Le, Lu Li, Chimezie Iwuanyanwu, Lu Liu, Kevin Ramirez, Andrey Khorlin, Albert Cui, Tian LIN, Marin Georgiev, Marcus Wu, Ricardo Aguilar, Keith Pallo, Abhishek Chakladar, Alena Repina, Xihui Wu, Tom van der Weide, Priya Ponnappalli, Caroline Kaplan, Jiri Simsa, Shuangfeng Li, Olivier Dousse, Fan Yang, Jeff Piper, Nathan Ie, Minnie Lui, Rama Pasumarathi, Nathan Lintz, Anitha Vijayakumar, Lam Nguyen Thiet, Daniel Andor, Pedro Valenzuela, Cosmin Paduraru, Daiyi Peng, Katherine Lee, Shuyuan Zhang, Somer Greene, Duc Dung Nguyen, Paula Kurylowicz, Sarmishta Velury, Sebastian Krause, Cassidy Hardin, Lucas Dixon, Lili Janzer, Kiam Choo, Ziqiang Feng, Biao Zhang, Achintya Singhal, Tejasi Latkar, Mingyang Zhang, Quoc Le, Elena Allica Abellan, Dayou Du, Dan McKinnon, Natasha Antropova, Tolga Bolukbasi, Orgad Keller, David Reid, Daniel Finchelstein, Maria Abi Raad, Remi Crocker, Peter Hawkins, Robert Dadashi, Colin Gaffney, Sid Lall, Ken Franko, Egor Filonov, Anna Bulanova, Rémi Leblond, Vikas Yadav, Shirley Chung, Harry Askham, Luis C. Cobo, Kelvin Xu, Felix Fischer, Jun Xu, Christina Sorokin, Chris Alberti, Chu-Cheng Lin, Colin Evans, Hao Zhou, Alek Dimitriev, Hannah Forbes, Dylan Banarse, Zora Tung, Jeremiah Liu, Mark Omernick, Colton Bishop, Chintu Kumar, Rachel Sterneck, Ryan Foley, Rohan Jain, Swaroop Mishra, Jiawei Xia, Taylor Bos, Geoffrey Cideron, Ehsan Amid, Francesco Piccinno, Xingyu Wang, Praseem Banzal, Petru Gurita, Hila Noga, Premal Shah, Daniel J. Mankowitz, Alex Polozov, Nate Kushman, Victoria Krakovna, Sasha Brown, MohammadHossein Bateni, Dennis Duan, Vlad Firoiu, Meghana Thotakuri, Tom Natan, Anhad Mohananey, Matthieu Geist, Sidharth Mudgal, Sertan Girgin, Hui Li, Jiayu Ye, Ofir Roval, Reiko Tojo, Michael Kwong, James Lee-Thorp, Christopher Yew, Quan Yuan, Sumit Bagri, Danila Sinopalnikov, Sabela Ramos, John Mellor, Abhishek Sharma, Aliaksei Severyn, Jonathan Lai, Kathy Wu, Heng-Tze Cheng, David Miller, Nicolas Sonnerat, Denis Vnukov, Rory Greig, Jennifer Beattie, Emily Caveness, Libin Bai, Julian Eisenschlos, Alex Korchemniy, Tomy Tsai, Mimi Jasarevic, Weize Kong, Phuong Dao, Zeyu Zheng, Frederick Liu, Fan Yang, Rui Zhu, Mark Geller, Tian Huey Teh, Jason Sanmiya, Evgeny Gladchenko, Nejc Trdin, Andrei Sozanschi, Daniel Toyama, Evan Rosen, Sasan Tavakkol, Linting Xue, Chen Elkind, Oliver Woodman, John Carpenter, George Papamakarios, Rupert Kemp, Sushant Kafle, Tanya Grunina, Rishika Sinha, Alice Talbert, Abhimanyu Goyal, Diane Wu, Denese Owusu-Afryie, Cosmo Du, Chloe Thornton, Jordi Pont-Tuset, Pradyumna Narayana, Jing Li, Sabaer Fatehi, John Wieting, Omar Ajmeri, Benigno Uribe, Tao Zhu, Yeongil Ko, Laura Knight, Amélie Héliou, Ning Niu, Shane Gu, Chenxi Pang, Dustin Tran, Yeqing Li, Nir Levine, Ariel Stolovich, Norbert Kalb, Rebeca Santamaria-Fernandez, Sonam Goenka, Wenny Yustalim, Robin Strudel, Ali Elqursh, Balaji Lakshminarayanan, Charlie Deck, Shyam Upadhyay, Hyo Lee, Mike Dusenberry, Zonglin Li, Xuezhi Wang, Kyle Levin, Raphael Hoffmann, Dan Holtmann-Rice, Olivier Bachem, Summer Yue, Sho Arora, Eric Malmi, Daniil Mirylenka, Qijun Tan, Christy Koh, Soheil Hassas Yeganeh, Siim Pöder, Steven Zheng, Francesco Pongetti, Mukarram Tariq, Yanhua Sun, Lucian Ionita, Mojtaba Seyedhosseini, Pouya Tafti, Raghav Kotikalapudi, Zhiyu Liu, Anmol Gulati, Jasmine Liu, Xinyu Ye, Bart Chrzaszcz, Lily Wang, Nikhil Sethi, Tianrun Li, Ben Brown, Shreya Singh, Wei Fan, Aaron Parisi, Joe Stanton, Chenkai Kuang, Vinod Koverkathu, Christopher A. Choquette-Choo, Yunjie Li, TJ Lu, Abe Ittycheriah, Prakash Shroff, Pei Sun, Mani Varadarajan, Sanaz Bahargam, Rob Willoughby, David Gaddy, Ishita Dasgupta, Guillaume Desjardins, Marco Cornero, Brona Robenek, Bhavishya Mittal, Ben Albrecht, Ashish Shenoy, Fedor Moiseev, Henrik Jacobsson,

Alireza Ghaffarkhah, Morgane Rivière, Alanna Walton, Clément Crepy, Alicia Parrish, Yuan Liu, Zongwei Zhou, Clement Farabet, Carey Radebaugh, Praveen Srinivasan, Claudia van der Salm, Andreas Fidjeland, Salvatore Scellato, Eri Latorre-Chimoto, Hanna Klimczak-Plucińska, David Bridson, Dario de Cesare, Tom Hudson, Piermaria Mendolicchio, Lexi Walker, Alex Morris, Ivo Penchev, Matthew Mauger, Alexey Guseynov, Alison Reid, Seth Odoom, Lucia Loher, Victor Cotruta, Madhavi Yenugula, Dominik Grewe, Anastasia Petrushkina, Tom Duerig, Antonio Sanchez, Steve Yadlowsky, Amy Shen, Amir Globerson, Adam Kurzrok, Lynette Webb, Sahil Dua, Dong Li, Preethi Lahoti, Surya Bhupatiraju, Dan Hurt, Haroon Qureshi, Ananth Agarwal, Tomer Shani, Matan Eyal, Anuj Khare, Shreyas Rammohan Belle, Lei Wang, Chetan Tekur, Mihir Sanjay Kale, Jinliang Wei, Ruoxin Sang, Brennan Saeta, Tyler Liechty, Yi Sun, Yao Zhao, Stephan Lee, Pandu Nayak, Doug Fritz, Manish Reddy Vuyyuru, John Aslanides, Nidhi Vyas, Martin Wicke, Xiao Ma, Taylan Bilal, Evgenii Eltyshv, Daniel Balle, Nina Martin, Hardie Cate, James Manyika, Keyvan Amiri, Yelin Kim, Xi Xiong, Kai Kang, Florian Luisier, Nilesh Tripuraneni, David Madras, Mandy Guo, Austin Waters, Oliver Wang, Joshua Ainslie, Jason Baldridge, Han Zhang, Garima Pruthi, Jakob Bauer, Feng Yang, Riham Mansour, Jason Gelman, Yang Xu, George Polovets, Ji Liu, Honglong Cai, Warren Chen, XiangHai Sheng, Emily Xue, Sherjil Ozair, Adams Yu, Christof Angermueller, Xiaowei Li, Weiren Wang, Julia Wiesinger, Emmanouil Koukoumidis, Yuan Tian, Anand Iyer, Madhu Gurumurthy, Mark Goldenson, Parashar Shah, MK Blake, Hongkun Yu, Anthony Urbanowicz, Jennimaria Palomaki, Chrisantha Fernando, Kevin Brooks, Ken Durden, Harsh Mehta, Nikola Momchev, Elahe Rahimtoroghi, Maria Georgaki, Amit Raul, Sebastian Ruder, Morgan Redshaw, Jinhyuk Lee, Komal Jalan, Dinghua Li, Ginger Perng, Blake Hechtman, Parker Schuh, Milad Nasr, Mia Chen, Kieran Milan, Vladimir Mikulik, Trevor Strohman, Juliana Franco, Tim Green, Demis Hassabis, Koray Kavukcuoglu, Jeffrey Dean, and Oriol Vinyals. Gemini: A family of highly capable multimodal models, 2023.

- [70] Neil Thomas and Lucy J. Colwell. Minding the gaps: The importance of navigating holes in protein fitness landscapes. *Cell Systems*, 12(11):1019–1020, 2021. ISSN 2405-4712. URL <https://www.sciencedirect.com/science/article/pii/S24054712211004154>.
- [71] Summer B. Thyme, Yifan Song, T. J. Brunette, Mindy D. Szeto, Lara Kusak, Philip Bradley, and David Baker. Massively parallel determination and modeling of endonuclease substrate specificity. *Nucleic Acids Res*, 42(22):13839–13852, December 2014. ISSN 0305-1048. URL <https://doi.org/10.1093/nar/gku1096>.
- [72] Hugo Touvron, Thibaut Lavril, Gautier Izacard, Xavier Martinet, Marie-Anne Lachaux, Timothée Lacroix, Baptiste Rozière, Naman Goyal, Eric Hambro, Faisal Azhar, Aurelien Rodriguez, Armand Joulin, Edouard Grave, and Guillaume Lample. Llama: Open and efficient foundation language models, 2023.
- [73] Hugo Touvron, Louis Martin, Kevin Stone, Peter Albert, Amjad Almahairi, Yasmine Babaei, Nikolay Bashlykov, Soumya Batra, Prajjwal Bhargava, Shrutu Bhosale, Dan Bikel, Lukas Blecher, Cristian Canton Ferrer, Moya Chen, Guillem Cucurull, David Esiobu, Jude Fernandes, Jeremy Fu, Wenyin Fu, Brian Fuller, Cynthia Gao, Vedanuj Goswami, Naman Goyal, Anthony Hartshorn, Saghar Hosseini, Rui Hou, Hakan Inan, Marcin Kardas, Viktor Kerkez, Madian Khabsa, Isabel Kloumann, Artem Korenev, Punit Singh Koura, Marie-Anne Lachaux, Thibaut Lavril, Jenya Lee, Diana Liskovich, Yinghai Lu, Yuning Mao, Xavier Martinet, Todor Mihaylov, Pushkar Mishra, Igor Molybog, Yixin Nie, Andrew Poulton, Jeremy Reizenstein, Rashi Rungta, Kalyan Saladi, Alan Schelten, Ruan Silva, Eric Michael Smith, Ranjan Subramanian, Xiaoqing Ellen Tan, Binh Tang, Ross Taylor, Adina Williams, Jian Xiang Kuan, Puxin Xu, Zheng Yan, Iliyan Zarov, Yuchen Zhang, Angela Fan, Melanie Kambadur, Sharan Narang, Aurelien Rodriguez, Robert Stojnic, Sergey Edunov, and Thomas Scialom. Llama 2: Open foundation and fine-tuned chat models, 2023.
- [74] Gerard Van Westen, Remco Swier, Joerg Wegner, Adriaan Ijzerman, Herman Vlijmen, and Andreas Bender. Benchmarking of protein descriptor sets in proteochemometric modeling (part 1): Comparative study of 13 amino acid descriptor sets. *Journal of cheminformatics*, 5:41, September 2013.
- [75] Rosario Vanella, Gordana Kovacevic, Vanni Doffini, Jaime Fernández de Santaella, and Michael A. Nash. High-throughput screening, next generation sequencing and machine learning:

- advanced methods in enzyme engineering. *Chem. Commun.*, 58(15):2455–2467, January 2022. ISSN 1359-7345. URL <http://dx.doi.org/10.1039/D1CC04635G>.
- [76] Rosario Vanella, Christoph Küng, Alexandre A. Schoepfer, Vanni Doffini, Jin Ren, and Michael A. Nash. Understanding activity-stability tradeoffs in biocatalysts by enzyme proximity sequencing. *Nature Communications*, 15(1):1807, 2024. ISSN 2041-1723. URL <https://doi.org/10.1038/s41467-024-45630-3>.
- [77] Valdimir N. Vapnik. *The Nature of Statistical Learning Theory*. Springer, second edition, 1995. doi: 10.1007/978-1-4757-3264-1.
- [78] Mihaly Varadi and Sameer Velankar. The impact of alphafold protein structure database on the fields of life sciences. *Proteomics*, 23(17):2200128, September 2023. ISSN 1615-9853. URL <https://doi.org/10.1002/pmic.202200128>.
- [79] T. Viering and M. Loog. The shape of learning curves: A review. *IEEE Transactions on Pattern Analysis and Machine Intelligence*, pages 1–20, 2022. ISSN 1939-3539.
- [80] O. Anatole von Lilienfeld, Klaus-Robert Müller, and Alexandre Tkatchenko. Exploring chemical compound space with quantum-based machine learning. *Nature Reviews Chemistry*, 4(7):347–358, 2020. ISSN 2397-3358. URL <https://doi.org/10.1038/s41570-020-0189-9>.
- [81] Kristof T. Schütt; Stefan Chmiela; O. Anatole von Lilienfeld; Alexandre Tkatchenko; Koji Tsuda; Klaus-Robert Müller; editor. *Machine Learning Meets Quantum Physics*. Springer, 2020.
- [82] Yi Wang, Hui Tang, Lichao Huang, Lulu Pan, Lixiang Yang, Huanming Yang, Feng Mu, and Meng Yang. Self-play reinforcement learning guides protein engineering. *Nature Machine Intelligence*, 5(8):845–860, 2023. ISSN 2522-5839. URL <https://doi.org/10.1038/s42256-023-00691-9>.
- [83] Timothy L. H. Watkin, Albrecht Rau, and Michael Biehl. The statistical mechanics of learning a rule. *RMP*, 65(2):499–556, April 1993. URL <https://link.aps.org/doi/10.1103/RevModPhys.65.499>.
- [84] Bruce J. Wittmann, Kadina E. Johnston, Zachary Wu, and Frances H. Arnold. Advances in machine learning for directed evolution. *Current Opinion in Structural Biology*, 69:11–18, 2021. ISSN 0959-440X. URL <https://www.sciencedirect.com/science/article/pii/S0959440X21000154>.
- [85] Bruce J. Wittmann, Yisong Yue, and Frances H. Arnold. Informed training set design enables efficient machine learning-assisted directed protein evolution. *Cell Systems*, 12(11):1026–1045.e7, 2021. ISSN 2405-4712. URL <https://www.sciencedirect.com/science/article/pii/S2405471221002866>.
- [86] Marcel Wittmund, Frederic Cadet, and Mehdi D. Davari. Learning epistasis and residue coevolution patterns: Current trends and future perspectives for advancing enzyme engineering. *ACS Catal.*, 12(22):14243–14263, November 2022. doi: 10.1021/acscatal.2c01426. URL <https://doi.org/10.1021/acscatal.2c01426>.
- [87] Yaning Xu, Fengxi Li, Hanqing Xie, Yuyang Liu, Weiwei Han, Junhao Wu, Lei Cheng, Chunyu Wang, Zhengqiang Li, and Lei Wang. Directed evolution of escherichia coli surface-displayed vitreoscilla hemoglobin as an artificial metalloenzyme for the synthesis of 5-imino-1,2,4-thiadiazoles. *Chem. Sci.*, pages –, 2024. doi: 10.1039/D4SC00005F. URL <http://dx.doi.org/10.1039/D4SC00005F>.
- [88] Andy Hsien-Wei Yeh, Christoffer Norn, Yakov Kipnis, Doug Tischer, Samuel J. Pellock, Declan Evans, Pengchen Ma, Gyu Rie Lee, Jason Z. Zhang, Ivan Anishchenko, Brian Coventry, Longxing Cao, Justas Dauparas, Samer Halabiya, Michelle DeWitt, Lauren Carter, K. N. Houk, and David Baker. De novo design of luciferases using deep learning. *Nature*, 614(7949):774–780, 2023. ISSN 1476-4687. URL <https://doi.org/10.1038/s41586-023-05696-3>.

## A Code and Data Availability Statement

The data and code produced for this work, including the documentation associated, are available free of charge on [10.5281/zenodo.11148308](https://zenodo.org/record/11148308) and <https://github.com/Nash-Lab/DiscontinuousLCs>.

## B Materials and Methods

### B.1 Database Generation

We calculated the number of specific and total possible mutations in a discretised space with fixed structure with equations (2) and (3).

$$D_{spec}^{disc}(n, p, v) = \binom{n}{p} \cdot (v - 1)^p \quad (2)$$

$$D_{tot}^{disc}(n, m, v) = \sum_{p=0}^m \binom{n}{p} \cdot (v - 1)^p \quad (3)$$

Where  $n$  is the number of positions allowed to mutate,  $p$  and  $m$  are the number of mutations, and  $v$  is the vocabulary size, i.e., the number of possible building blocks that can be drawn. It should be noted that these equations hold true exclusively under the condition that all constituent building blocks (whether amino acids or atoms) of the initial sequence (WT) are included in the vocabulary. Should a scenario arise where none of these components are present, a simplification of the equations can be achieved by discarding the “-1” term. For scenarios that fall between these extremes, it becomes necessary to formulate more specialized and less intuitive expressions tailored to each specific case. The equations in question were utilized to evaluate the feasibility of creating in-silico libraries encompassing both a biological and a chemical system. For the biological system, we chose a segment of the modified Fg- $\beta$  peptide (*FFFSARG*,  $n = 7$ ) to be the WT (Fig. 2A.1). This specific sequence was previously characterized by Ponnuraj et al. [52]. During the main study, we limited the vocabulary to the amino acids already present in the initial sequence ( $v = 5$ ), namely: Alanine (A), Phenylalanine (F), Glycine (G), Arginine (R) and Serine (S). This allowed us to generate an unlabelled database of possible mutations (Fig. 2A.2). Furthermore, to enhance the robustness of our study, we expanded our analysis to incorporate Cysteine (C), due to the inclusion of a sulfur atom; Aspartic acid (D), attributed to its negatively charged side chain; and Tryptophan (W), which is distinguished as the largest and heaviest amino acid. For the chemical system, the selection was made on hexane ( $C_6H_{14}$ ,  $n = 6$ ) and cyclohexane ( $C_6H_{12}$ ,  $n = 6$ ), allowing the substitution of the carbon atoms with oxygen(s) or nitrogen(s). The hybridisation was fixed to Sp3 and the structures were filled accordingly with hydrogen atoms. It should be noted that, given molecules typically exhibit linear or nonlinear graph-based structures lacking a clear direction of interpretation, certain mutations were functionally equivalent due to symmetries. However, for simplicity, these equivalences were disregarded in our study.

A summary of the number of mutants is provided in Supporting Table S1.

Table S1: Size of mutagenised databases generated. The top part refers to the specific mutations (WT, single, double, etc.), while the bottom, correspond to the cumulative number of mutations (WT, WT+single, WT+single+double, etc.).

Database	$m=0$	$m=1$	$m=2$	$m=3$	$m=4$	$m=5$	$m=6$	$m=7$
Fg- $\beta$	1	28	336	2240	8960	21504	28672	16384
Fg- $\beta$ Ext.	1	49	1029	12005	84035	352947	823543	823543
Chem. Space	2	24	120	320	480	384	128	-
Fg- $\beta$	1	29	365	2605	11565	33069	61741	78125
Fg- $\beta$ Ext.	1	50	1079	13084	97119	450066	1273609	2097152
Chem. Space	2	26	146	466	946	1330	1458	-



Table S2: Parameters of dictionaries  $g_1\{\cdot\}$  and  $g_2\{\cdot\}$ .

Key	z=1	z=2
$g_z\{A\}$	0.548	0.417
$g_z\{F\}$	0.715	0.720
$g_z\{G\}$	0.602	0.000
$g_z\{R\}$	0.544	0.302
$g_z\{S\}$	0.423	0.146
$g_z\{C\}$	0.645	0.092
$g_z\{D\}$	0.437	0.186
$g_z\{W\}$	0.891	0.345

We employed different functions to label our generated databases. In the peptide case, we started with two functions inspired by the many-body theory from quantum physics [81]. To maintain the initial analysis as a proof of concept, we implemented the following simplifications: (i) amino acids were utilized as the primary units for computation, thereby avoiding a reduction to the atomic level; (ii) the spatial separation between distinct units was quantified using the integer difference in their positions, as described in equation (6); and (iii) the hash maps  $g_1\{\cdot\}$  and  $g_2\{\cdot\}$  (Tab. S2), assigning a unique number to each amino acid in the vocabulary, were established through random sampling rather than derived from physico-chemical properties. This last approach was chosen to preclude any potential bias that might arise from prioritizing one chemical/physical attribute over another. The mechanisms underlying one-body and two-body terms interactions were encapsulated by equations (4) and (5), respectively.

$$f_{1body}(x) = \sum_{k=1}^{L_x} g_1\{x_k\} \quad (4)$$

$$f_{2body}(x) = \sum_{k=1}^{L_x} g_1\{x_k\} + \sum_{i=1}^{L_x-1} \sum_{j=i+1}^{L_x} \frac{g_2\{x_i\} \cdot g_2\{x_j\}}{d(i, j)} \quad (5)$$

Where  $x$  is a peptide,  $x_{k/i/j}$  is the amino acid of  $x$  at position  $k$ ,  $i$  or  $j$ , and  $d$  is the distance between the different amino acids (eq. 6).

$$d(i, j) = |j - i| \quad (6)$$

Subsequently, we utilized EvoDesign physical Energy Function (EvoEF), a composite energy force field developed by the Zhang group [50, 31]). Specifically, we used EvoEF1 to estimate the binding energies between the mutagenised Fg- $\beta$  peptides contained in our database and SdrG protein (Algorithm 1 and Fig. 2A.3). This corresponded to chains C and A contained in the Protein Data Bank (PDB) database, file 1r17 [52], while chains D and B remained unaltered throughout the computational process. To decrease the running time, the loop was divided in 512 instances, which were run in parallel on our computer cluster.

**Data:** 1r17.pdb

**Result:** *energy*

*1r17\_Repair*  $\leftarrow$  *RepairStructure*(1r17);

**for**  $m \leftarrow 0$  **to**  $M$  **do**

*1r17\_Repair\_Mut*  $\leftarrow$  *BuildMutant*(1r17\_Repair);

*E<sub>Evo</sub>*  $\leftarrow$  *ComputeBinding*(1r17\_Repair\_Mut\_Repair);

**end**

**Algorithm 1:** EvoEF1 energy calculation

Regarding our molecular constructs, we calculated the corresponding solvation energies in water at a fixed temperature of 298 K for each compound contained within the database. To estimate such

energies we employed the leruli library [21], which utilized the works of Bell et al. [9] and Chung et al. [17].

## B.2 Encoding

During this study we mainly employed flattened One Hot Encoding (OHE, Fig. 2B) to translate each of our sequences, whether they were constituted by amino acids in a peptide or atoms in a molecule, in a unique, sparse and binary tensor. Even if one had to renounce completely on any physico-chemical information, such representation is still broadly used in the scientific community focused on biological macromolecules and present few advantages. Firstly, the input data could be structured in the same way for both peptides or molecules, making it possible to compare our observations across different topics. Secondly, the process did not require three-dimensional structural data, thus circumventing the need for costly and potentially imprecise simulations [37, 38], particularly relevant in the context of peptide-protein interactions. Thirdly, it was not reliant on any pre-trained ML model [40, 3, 48] or evolutionary/alignment (MSA) strategy [13, 34], rendering it well suitable for localized DMS datasets.

When integrating the linear and cyclic molecular graphs, we augmented the OHE matrix by appending an additional column. This column contained a zero for rows corresponding to linear structures and a one for all others, effectively distinguishing between the two molecular configurations.

In addition to OHE, our research was expanded to include a variety of other encoding techniques. For the mutagenized peptides, we utilized a binned version of the z-score, presented by Van Westen et al. [74], and a reduced version of the popular amino acids index database (AA index) [36]. The first alternative encoding, involved categorizing five physico-chemical properties (lipophilicity, size, polarity, electronegativity, and electrophilicity) into bins (Tab. S3). This process yielded a binary tensor analogous to OHE, with the distinction of retaining some degree of the physico-chemical information. The second method, consisted in compressing the AA index to 18 variables per amino acid through the application of principal component analysis (PCA) for dimensionality reduction (Tab. S4). Moreover, each variable was normalized utilizing a min-max scaling approach to ensure uniformity in the encoding scale. Regarding our molecular constructs, they were also represented through encoding with the standard flattened Coulomb matrix [60] (eq. 7), in addition to a variation of this matrix that was sorted according to eigenvalues [43].

$$M_{ij} = \begin{cases} \frac{1}{2} Z_i^{2.4} & \text{if } i = j \\ \frac{Z_i Z_j}{\|r_i - r_j\|_2} & \text{if } i \neq j \end{cases} \quad (7)$$

Where  $i$  and  $j$  are indices of the atoms in the encoded molecule,  $Z$  is the nuclear charge and  $r$  contains the atomic spatial coordinates.

## B.3 Machine Learning

Kernel ridge regression (KRR) [77, 56, 19, 29] was employed as the sole ML algorithm throughout the study (Fig. 2C). One of the primary advantages of this non-parametric method is its closed-form solution (eq. 8).

$$\alpha = (K(x_{i \in \text{train}}, x_{j \in \text{train}}) + \lambda I)^{-1} y_{\text{train}} \quad (8)$$

Where  $K$  denotes the Laplacian shift-invariant kernel (eq. 9). The variables  $x_{i/j}$  are the rows associated with the instances of the training set within the flattened OHE matrix (Fig. 2B). The vector  $y_{\text{train}}$  contains the labels corresponding to the training set. Furthermore,  $I$  is the identity matrix and  $\lambda$  is the estimation of the label error. For computational stability reasons,  $\lambda$  was set equal to  $1 \cdot 10^{-8}$ . The matrix inversion was handled via Cholesky decomposition [1].

$$K_{ij} = K(x_i, x_j) = \exp\left(-\frac{\|x_i - x_j\|_1}{\sigma}\right) \quad (9)$$

The hyperparameter  $\sigma$  was optimized by grid search, calculating the MAE on a validation set (eq. 10).

$$\sigma^* = \arg \min_{\sigma} \frac{1}{N_{valid}} \sum_{i \in valid} \left| y_i - \sum_{j \in train} K_{ij} \alpha_j \right| \quad (10)$$

Upon determining the optimal scale of the kernel, it could then be applied to predict the response variable for new data points (eq. 11).

$$\hat{y}_i = \sum_{j \in train} \exp\left(-\frac{\|x_i - x_j\|_1}{\sigma^*}\right) \alpha_j \quad (11)$$

To calculate the Manhattan distance in the Laplacian kernel (eq. 9) we exploited the inherent property of the OHE matrix, which consists exclusively of binary values. This property resulted in the Manhattan distance being equivalent to the square of the Euclidean distance ( $d_e^2$ ), thereby enabling its computation through the use of the inner product (eq. 12).

$$\|x_i - x_j\|_1 = d_e^2 = \langle x_i, x_i \rangle + \langle x_j, x_j \rangle - 2\langle x_i, x_j \rangle \quad (12)$$

In this study, two distinct strategies were employed for kernel shuffling (Fig. S1). The first approach, called random-based shuffling, involved the creation of an index vector with a dimension identical to that of the entire kernel matrix (encompassing all data points). This vector was subsequently randomly shuffled and utilized to reorder both the rows and columns of the kernel matrix accordingly. The second strategy, referred as mutant-based shuffling, also utilized a randomly shuffled index vector, similar to the first method. However, prior to employing this vector for reordering the rows and columns, the indices were rearranged based on the mutations present in the corresponding data points. This approach effectively randomizes the positioning of data points within groups defined by a specific number of mutations. For the implications of shuffling on the composition of training, validation and test set, refer to the following section.

#### B.4 Evaluation

To assess the performance of our models, we employed two methodologies: the generation of calibration plots and the analysis of learning curves (LCs, Fig. 2D). Both strategies were applied to independent test sets. The first technique involved plotting the predicted fitness values ( $\hat{y}$ ) against the true (or "actual") fitness values ( $y$ ), and it was exclusively applied to evaluate the EvoEF case. For the LCs, we developed a new scaling strategy to enclose the combinatorial nature of our sets (Fig. 1). This was based on the idea that, data enclosing different numbers of mutations provided different amount of information to the ML model. To establish our novel scale, it was imperative to transcend the discrete boundary imposed by equations 2 and 3, allowing for inputs coming from the set of positive real numbers (eq. 13).

$$D_{tot}^{cont}(n, \hat{m}, v) = \sum_{p \in S(\hat{m})} \binom{n}{p}_{\Gamma(\cdot)} (v-1)^p \quad (13)$$

This was achieved by substituting the factorial operator by the gamma function in the binomial coefficient (eq. 14).

$$\binom{n}{p}_{\Gamma(\cdot)} = \frac{\Gamma(n+1)}{\Gamma(p+1) \cdot \Gamma(n-p+1)} \quad (14)$$

Moreover,  $p$  is defined over the set  $S$  (eq. 15), which depends on  $\hat{m}$ . It is noteworthy that  $\hat{m}$  can now assume any real, positive value that is equal to or less than  $n$ , overcoming the limit of equations 2 and 3.

$$S = \{p \in \mathbb{R} \mid p = \hat{m} - i, i \in \mathbb{N}_0, i \leq \hat{m} + 1\} \quad (15)$$

Finally, equation 13 can be applied to normalize an arbitrary number of data points ( $N$ ) by addressing an optimization problem (eq. 16) to derive a normalized variant of it ( $N^{norm}$ ), which was ultimately used in the LCs.

$$N^{norm} = \arg \min_{\hat{m} \in [0, n] \subset \mathbb{R}} (N - D_{tot}^{cont}(n, \hat{m}, v)) \quad (16)$$

In this research,  $N^{norm}$  was utilized to index the rows of the Laplacian kernel derived from the entire dataset. Unless explicitly indicated, the training set was delineated as  $N^{norm}$  values ranging from 0.0 to 3.0, the validation set encompassed all data points with  $N^{norm} \in (3.0, 4.0]$ , and the test set included those within  $N^{norm} \in (4.0, 5.0]$ . The choice of shuffling strategy—mutant-based versus randomly-based shuffling—influenced the potential limitation on the dataset composition to a certain subset of mutation numbers (Fig. S1). Specifically, employing mutant-based shuffling meant that the validation and test sets were exclusively comprised of quadruple ( $m = 4$ ) and quintuple ( $m = 5$ ) mutants, respectively. Conversely, with full random shuffling, each subset (training, validation, and test) could contain any mutation number.

## C Supporting Figures

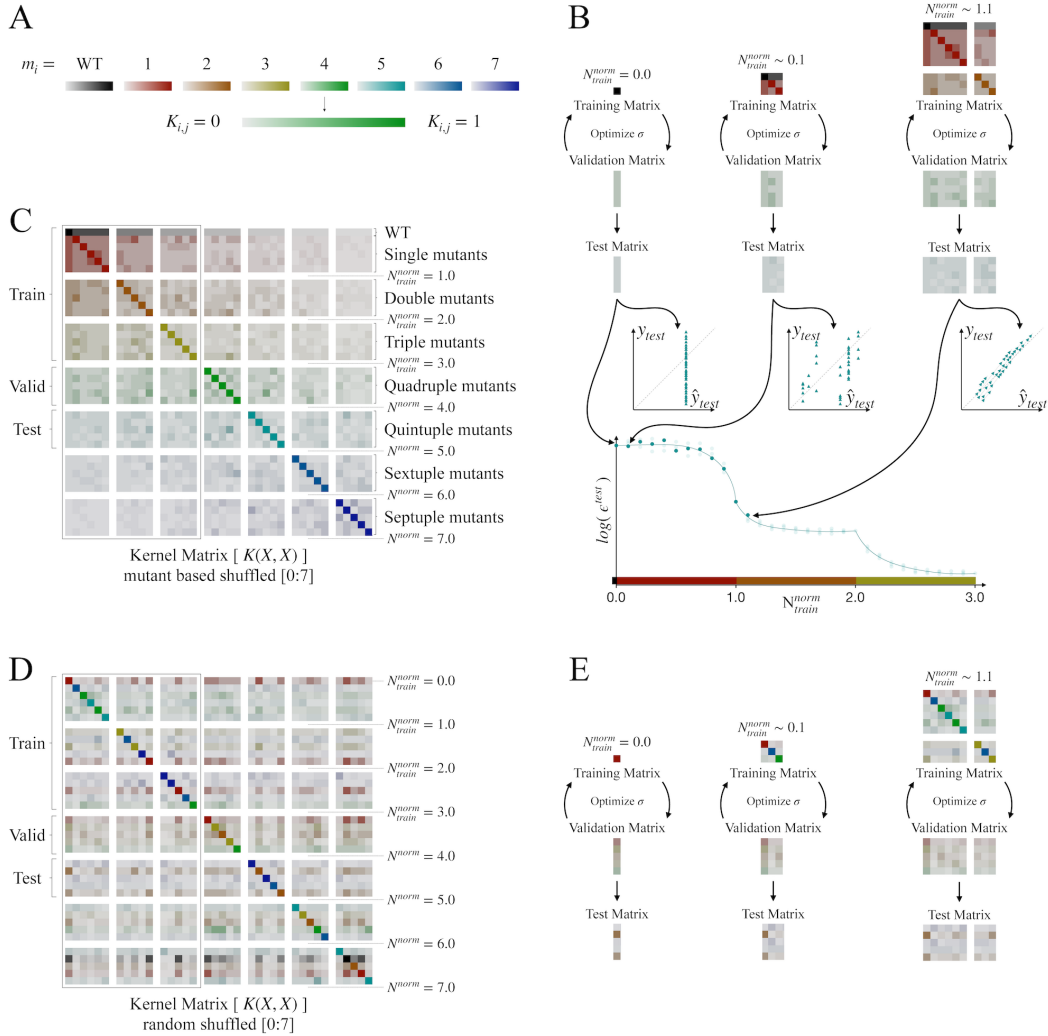


Figure S1: Extension on kernel shuffling techniques. (A) Color scheme (row wise): each variant with a specific number of mutations was colored accordingly. The color gradient (light grey – color) follows the specific kernel value (0 - 1). (B) Three examples of training – validation – test pipeline, including LCs and calibration plots, of fully mutant based shuffled kernel (C). (E) Three examples of training – validation – test pipeline of fully random shuffled kernel (D).

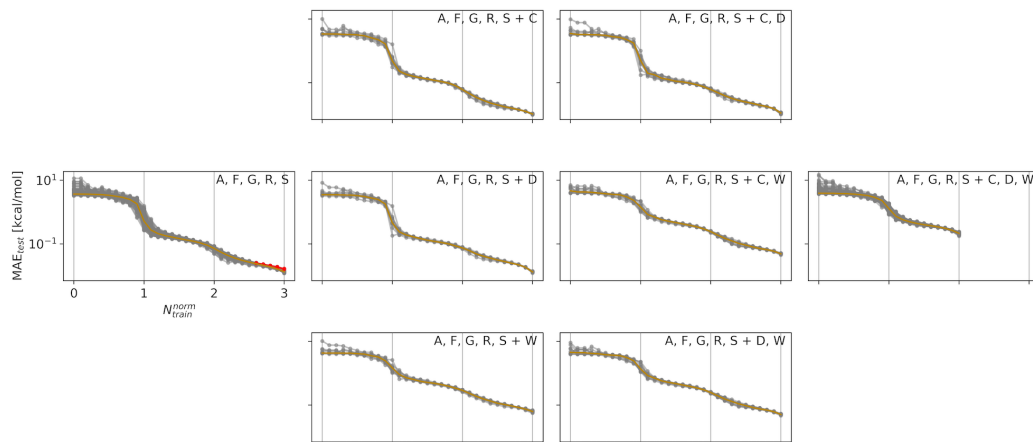


Figure S2: LCs predicting data generated with EvoEF function with variable vocabulary (black dots). The random-based shuffling was used across the whole dataset.

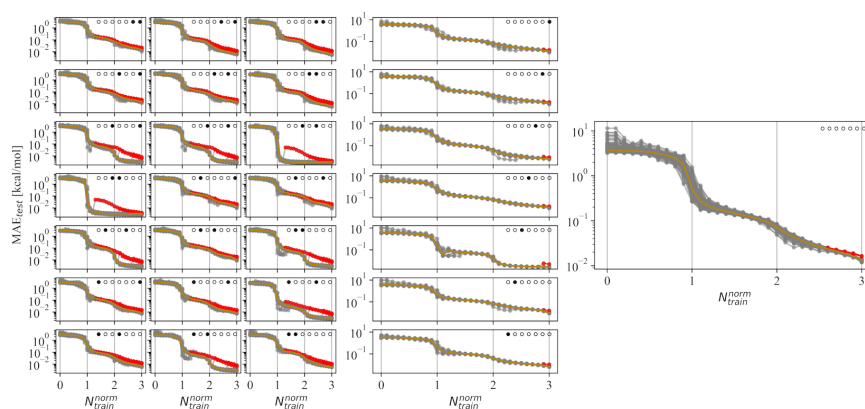


Figure S3: LCs predicting data generated with EvoEF function with unmutagenised positions (black dots). The left side contains all combinations with 5 variable sites ( $n=7$ ), the central panel contains all combinations with 6 variable sites ( $n=7$ ) and the right side shows the data reported in the main text. The random-based shuffling was used across the whole dataset.

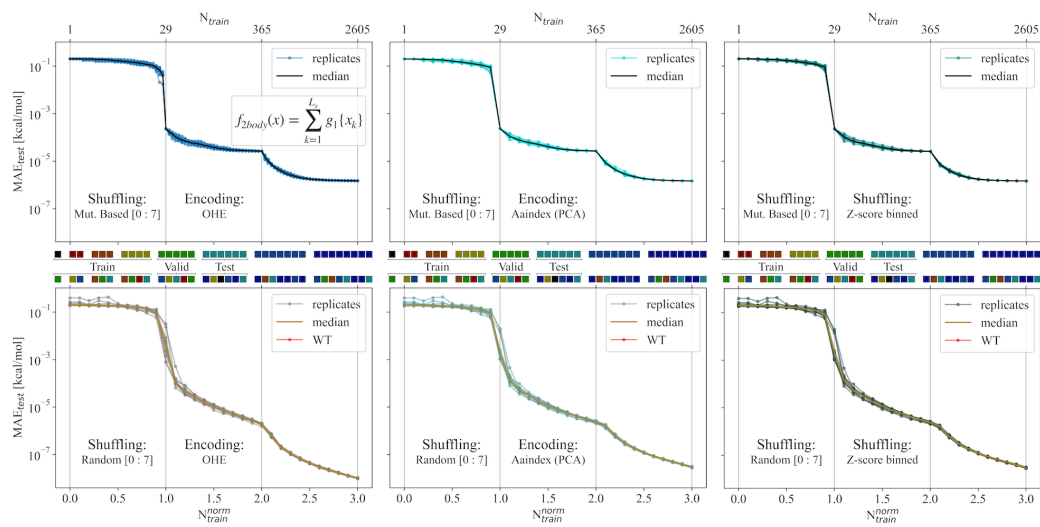


Figure S4: LCs predicting data generated with 1-body-term function with different shuffling (rows) and encoding (columns).



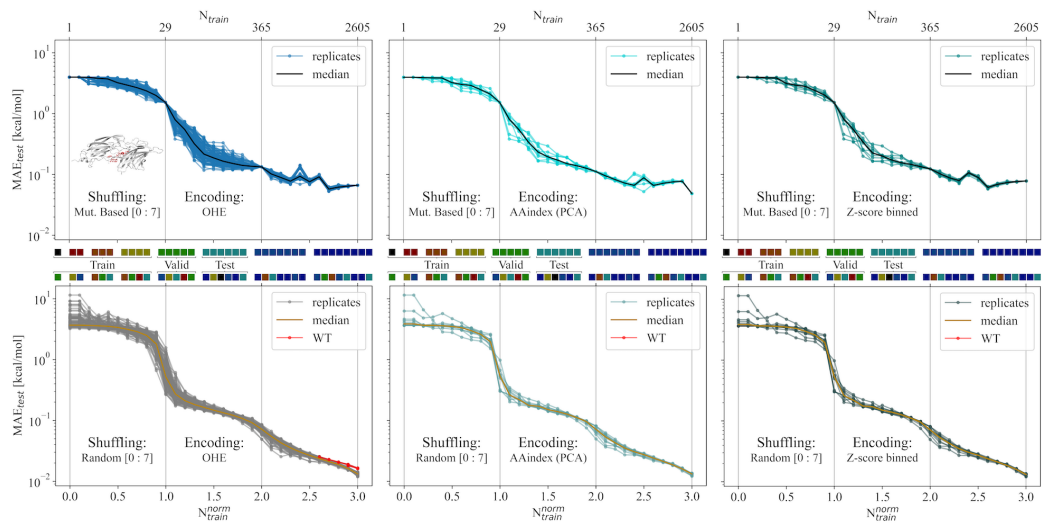


Figure S5: LCs predicting data generated with EvoEF function with different shuffling (rows) and encoding (columns).

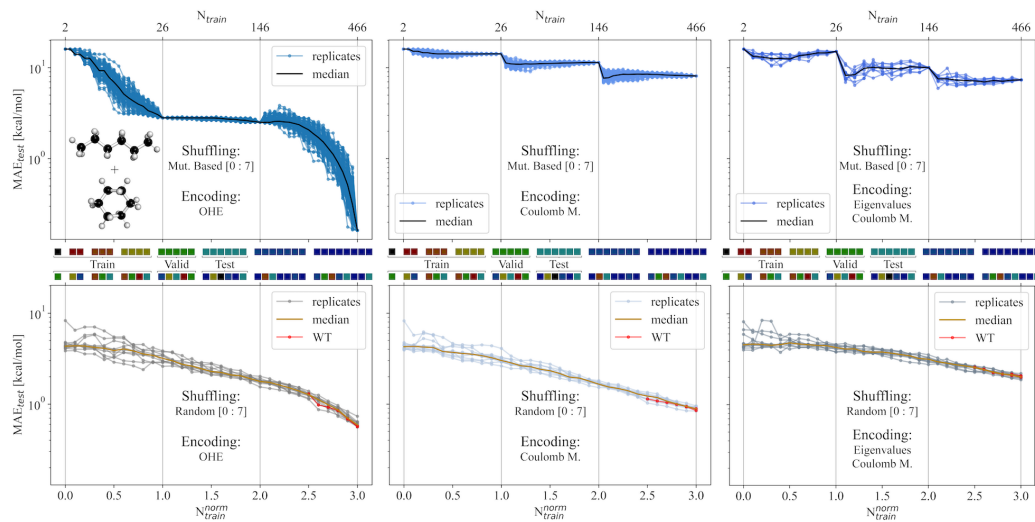


Figure S6: LCs predicting free solvation energies of the molecular database containing the linear (WT = hexane) and cyclic (WT = cyclohexane) graphs with different shuffling (rows) and encoding (columns).

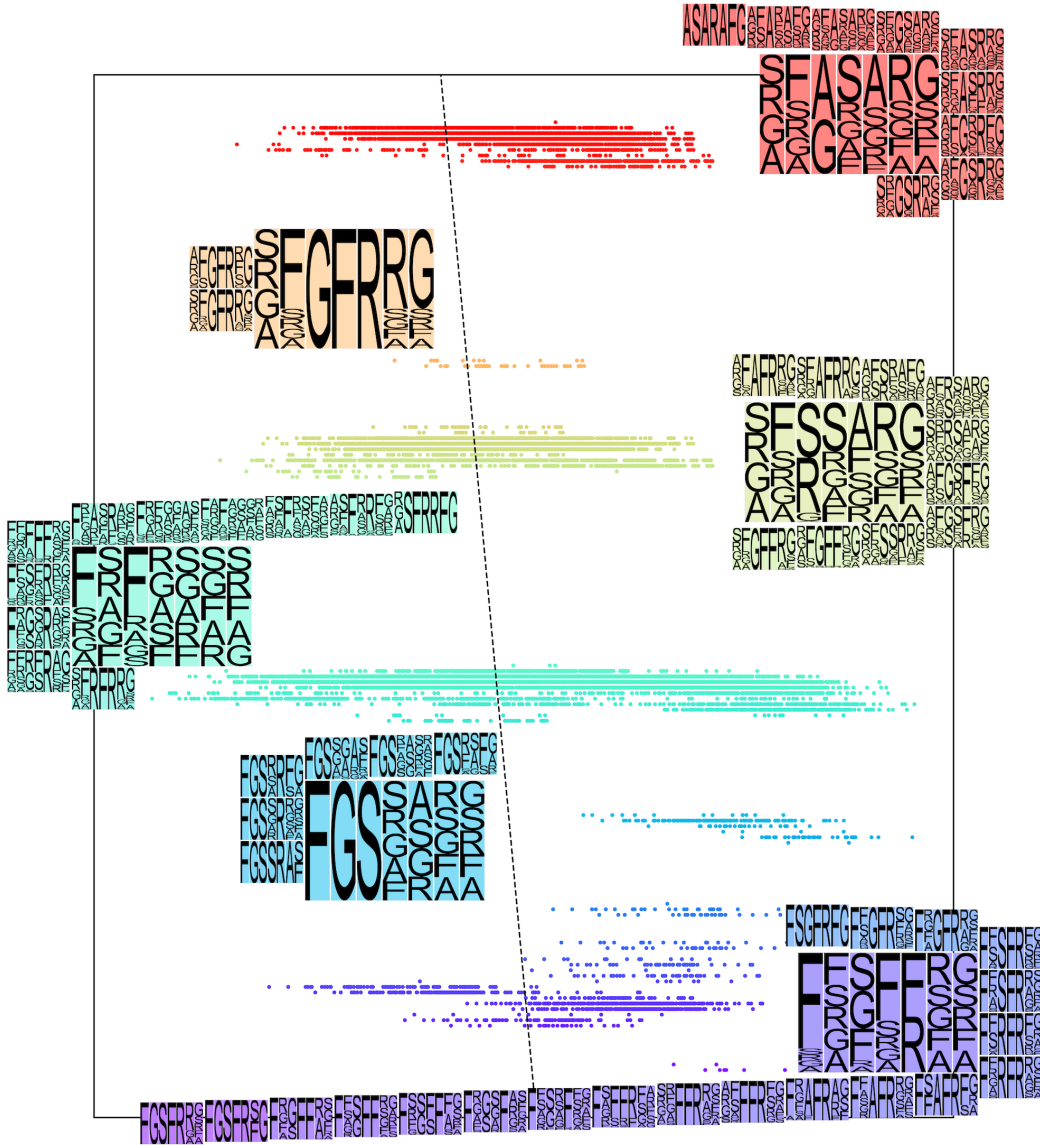


Figure S7: Extension on frequency distribution of amino acids when WT and all single mutants were included in the training set and all quintuple mutants were in the test set (Fig. 4B). The frequency distributions of all horizontal clusters were included as insets.

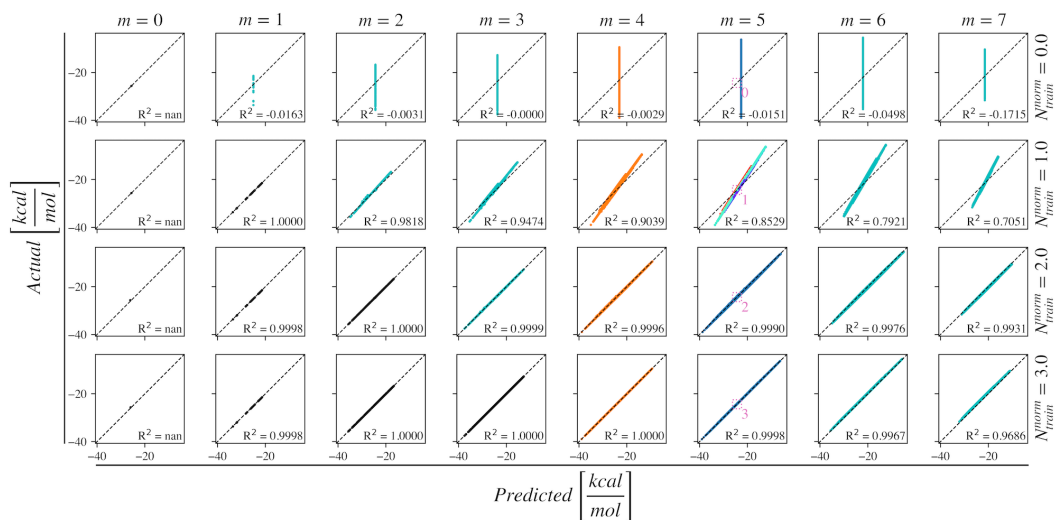


Figure S8: Extension on calibration plots of Fg-β / S. epidermidis adhesin SdrG complex binding energy function (EvoEF). Scatter plots showing actual vs. predicted energies. The columns correspond to different numbers of mutations ( $m$ ) while the rows correspond to the number of training examples provided ( $N_{train}^{norm} = 0.0$  - WT,  $N_{train}^{norm} = 1.0$  - WT plus single mutants, etc.). Color scheme: black dots - training set, orange dots - validation set, blue / rainbow dots - test set containing quintuple mutations (standard used across this work for mutant-based shuffling), cyan dots - test sets containing other mutations.

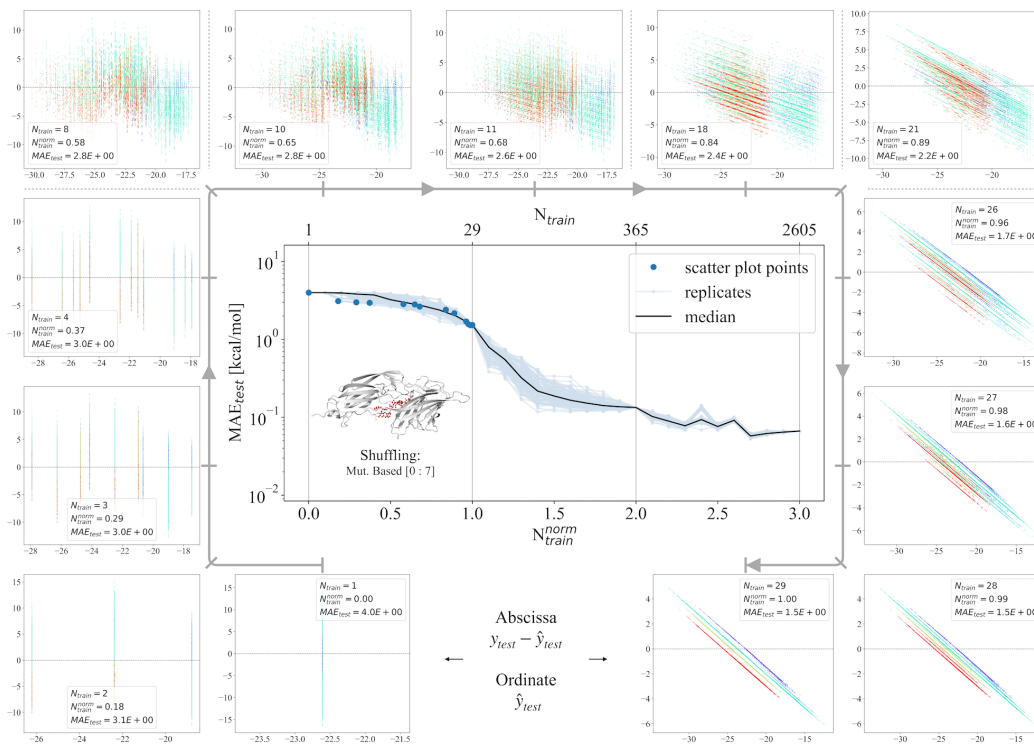


Figure S9: Error vs. predicted extension on data generated with EvoEF function (WT and single mutants) at different training instances. The central plot shows all LCs (100 replicates) and the specific points at which the analysis was carried (same replicate). The colormap is based on the clusters at the point where WT and all single mutants were included in the training set.

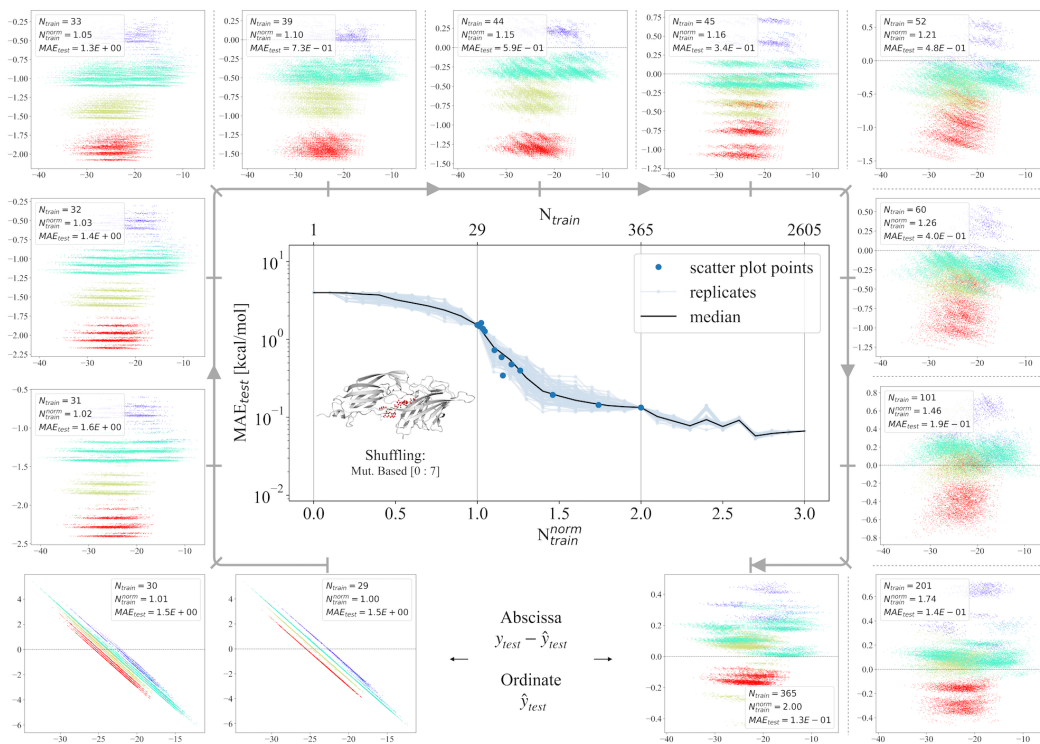


Figure S10: Error vs. predicted extension on data generated with EvoEF function (double mutants) at different training instances. The central plot shows all LCs (100 replicates) and the specific points at which the analysis was carried (same replicate). The colormap is based on the clusters at the point where WT and all single mutants were included in the training set.

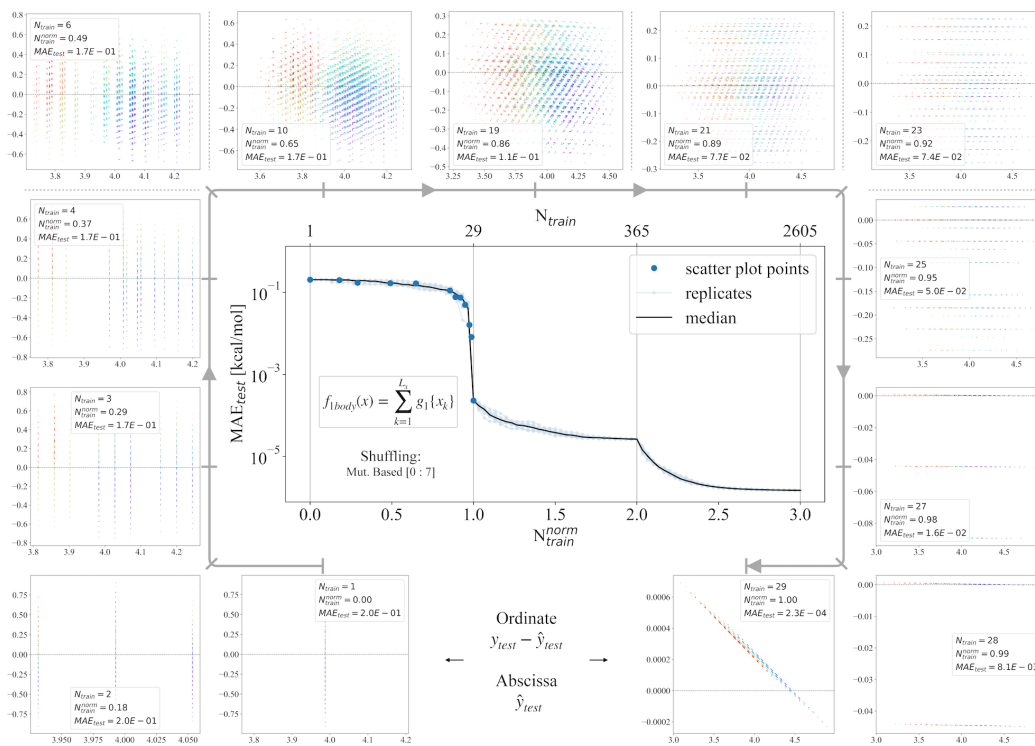


Figure S11: Error vs. predicted extension on data generated with 1-body term function (WT and single mutants) at different training instances. The central plot shows all LCs (100 replicates) and the specific points at which the analysis was carried out (same replicate). The colormap is based on the clusters at the point where WT and all single mutants were included in the training set.

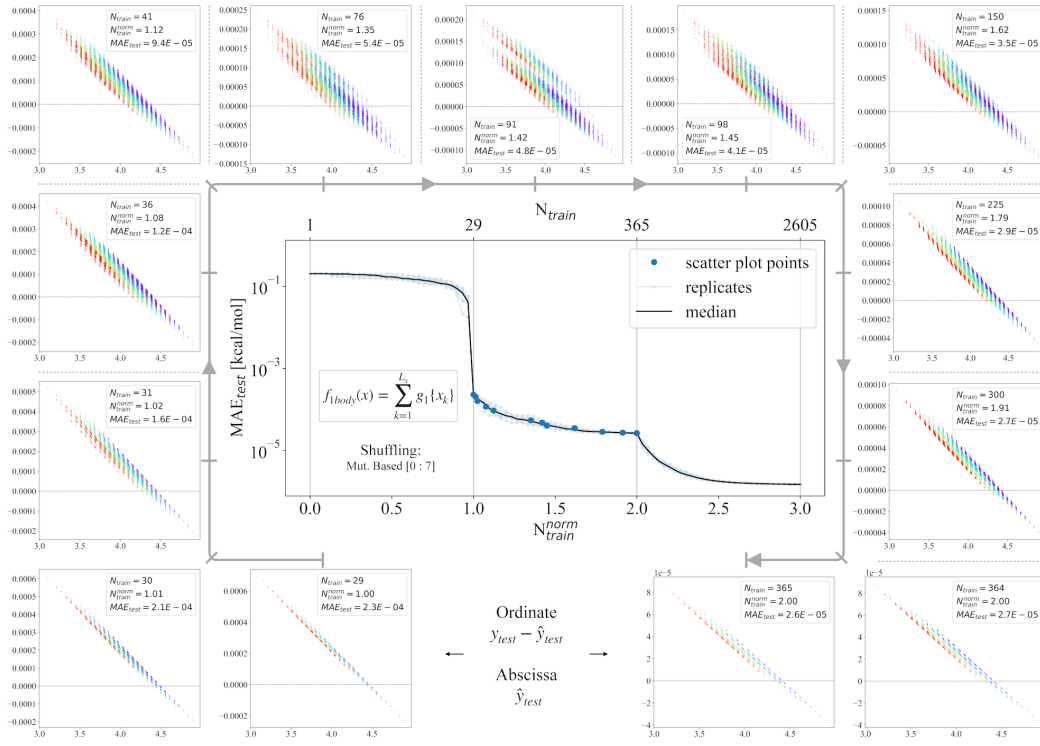


Figure S12: Error vs. predicted extension on data generated with 1-body term function (double mutants) at different training instances. The central plot shows all LCs (100 replicates) and the specific points at which the analysis was carried (same replicate). The colormap is based on the clusters at the point where WT and all single mutants were included in the training set.



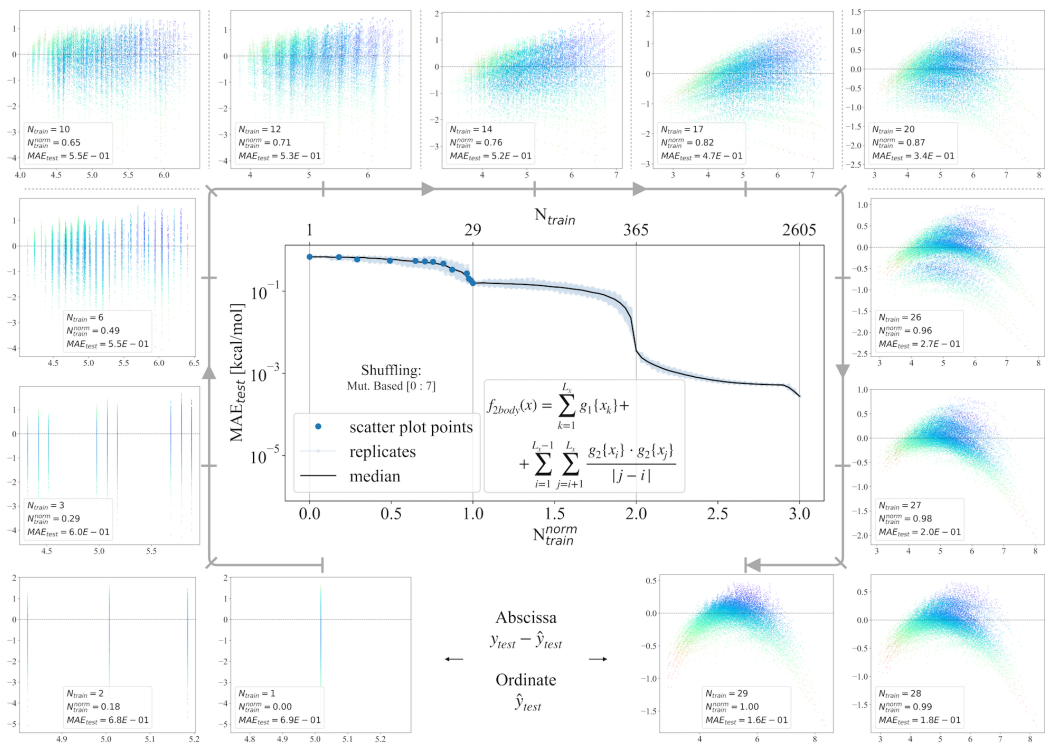


Figure S13: Error vs. predicted extension on data generated with 2-body term function (WT and single mutants) at different training instances. The central plot shows all LCs (100 replicates) and the specific points at which the analysis was carried (same replicate). The colormap is based on the clusters at the point where WT and all single mutants were included in the training set.

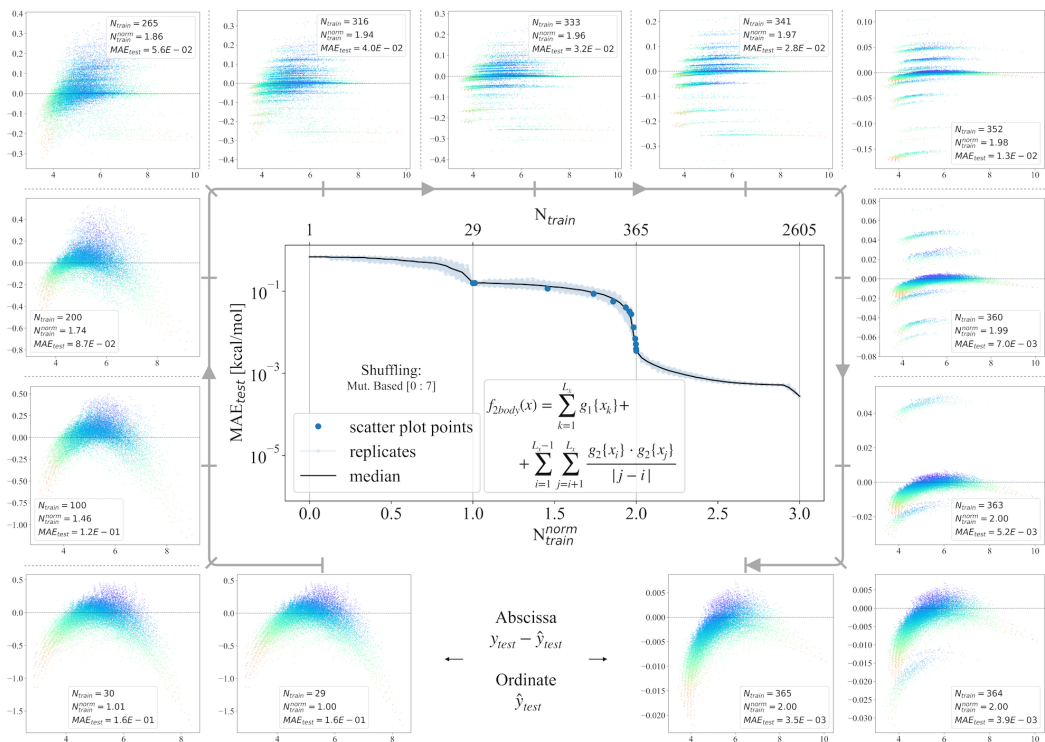


Figure S14: Error vs. predicted extension on data generated with 2-body term function (double mutants) at different training instances. The central plot shows all LCs (100 replicates) and the specific points at which the analysis was carried (same replicate). The colormap is based on the clusters at the point where WT and all single mutants were included in the training set.

## D Supporting Tables

Table S3: Z-score binned dictionary.

AA	Lipophilicity				Size				Polarity			Electronegativity				Electrophilicity			
	-	-	+	++	-	-	+	++	-	+	++	-	-	+	++	-	-	+	++
A	0	0	1	0	1	0	0	0	0	0	1	0	1	0	0	0	0	0	1
C	0	0	1	0	0	1	0	0	0	0	1	0	0	1	0	1	0	0	0
D	1	0	0	0	0	0	1	0	0	0	1	1	0	0	0	0	0	1	0
E	1	0	0	0	0	0	1	0	0	1	0	1	0	0	0	0	1	0	0
F	0	0	0	1	0	0	0	1	0	0	1	0	0	1	0	0	1	0	0
G	1	0	0	0	1	0	0	0	0	0	1	0	1	0	0	0	1	0	0
H	1	0	0	0	0	0	0	1	0	0	1	0	0	0	1	0	0	1	0
I	0	0	0	1	0	1	0	0	1	0	0	0	1	0	0	0	0	1	0
K	1	0	0	0	0	0	1	0	1	0	0	0	0	1	0	0	0	1	0
L	0	0	0	1	0	1	0	0	0	1	0	0	1	0	0	0	0	1	0
M	0	0	0	1	0	1	0	0	0	0	1	0	0	0	1	0	1	0	0
N	1	0	0	0	0	0	1	0	0	0	1	0	1	0	0	0	0	0	1
P	0	1	0	0	0	0	1	0	0	0	1	0	0	1	0	0	0	0	1
Q	0	0	1	0	0	0	1	0	0	1	0	1	0	0	0	0	0	1	0
R	1	0	0	0	0	0	0	1	1	0	0	0	0	0	1	0	1	0	0
S	1	0	0	0	0	1	0	0	0	0	1	1	0	0	0	0	0	1	0
T	0	0	1	0	1	0	0	0	0	1	0	1	0	0	0	0	1	0	0
V	0	0	0	1	1	0	0	0	0	1	0	0	1	0	0	0	1	0	0
W	0	0	0	1	0	0	0	1	0	0	1	0	0	0	1	1	0	0	0
Y	0	0	0	1	0	0	0	1	0	0	1	0	1	0	0	1	0	0	0

Table S4: AAindex PCA reduced (18 principal components) dictionary. Each column was normalized by a min-max scaler.

AA	PC0 34.4%	PC1 15.8%	PC2 11.7%	PC3 7.0%	PC4 5.5%	PC5 4.5%	PC6 3.2%	PC7 2.5%	PC8 2.2%	PC9 2.1%	PC10 1.9%	PC11 1.8%	PC12 1.5%	PC13 1.2%	PC14 1.1%	PC15 1.1%	PC16 1.0%	PC17 0.7%
A	0.476	0.574	1.000	0.479	0.629	0.590	0.210	0.352	0.624	0.242	0.511	0.568	0.520	0.626	0.981	0.853	0.645	0.181
R	0.261	0.000	0.432	0.453	0.000	0.012	0.237	0.036	0.141	0.000	0.863	0.308	0.200	0.464	0.647	0.419	0.418	0.415
N	0.080	0.421	0.335	0.272	0.354	0.658	0.601	0.753	0.317	0.720	0.605	0.313	0.006	0.104	1.000	0.484	0.321	0.231
D	0.000	0.344	0.466	0.381	0.761	0.788	1.000	0.304	0.156	0.303	0.545	0.357	0.123	1.000	0.185	0.471	0.695	0.403
C	0.681	0.642	0.238	0.000	1.000	0.000	0.325	0.070	0.218	0.678	0.635	0.494	0.477	0.419	0.401	0.487	0.424	0.351
Q	0.269	0.179	0.526	0.430	0.531	0.339	0.367	0.424	0.366	0.420	0.000	0.212	0.542	0.000	0.407	0.302	1.000	0.466
E	0.161	0.110	0.829	0.522	0.886	0.678	0.737	0.180	0.104	0.321	0.442	0.616	0.644	0.076	0.531	0.351	0.000	0.486
G	0.050	1.000	0.512	0.285	0.034	1.000	0.076	0.119	0.019	0.269	0.343	0.482	0.411	0.345	0.289	0.316	0.385	0.415
H	0.462	0.199	0.310	0.305	0.504	0.520	0.172	1.000	0.067	0.193	0.585	1.000	0.461	0.546	0.417	0.291	0.547	0.439
I	1.000	0.579	0.556	0.552	0.312	0.366	0.688	0.395	0.000	0.481	0.182	0.550	0.000	0.389	0.645	0.374	0.426	0.392
L	0.929	0.510	0.836	0.634	0.382	0.587	0.413	0.452	0.464	0.722	1.000	0.332	0.483	0.488	0.296	0.000	0.537	0.327
K	0.171	0.063	0.653	0.491	0.139	0.365	0.152	0.321	0.414	1.000	0.192	0.618	0.298	0.718	0.144	0.656	0.276	0.412
M	0.885	0.295	0.569	0.372	0.815	0.590	0.000	0.619	0.190	0.198	0.142	0.000	0.245	0.758	0.512	0.336	0.124	0.422
F	0.968	0.410	0.339	0.515	0.394	0.713	0.476	0.551	0.225	0.306	0.710	0.312	0.379	0.091	0.000	1.000	0.423	0.562
P	0.039	0.722	0.000	1.000	0.841	0.266	0.204	0.399	0.261	0.438	0.472	0.476	0.350	0.476	0.537	0.453	0.400	0.399
S	0.146	0.638	0.511	0.339	0.339	0.317	0.550	0.616	0.850	0.403	0.532	0.329	0.506	0.594	0.641	0.421	0.317	1.000
T	0.344	0.583	0.473	0.398	0.316	0.127	0.695	0.571	0.923	0.080	0.291	0.474	0.376	0.362	0.042	0.375	0.207	0.000
W	0.921	0.187	0.045	0.437	0.502	0.965	0.383	0.000	1.000	0.344	0.356	0.678	0.196	0.420	0.629	0.321	0.446	0.482
Y	0.683	0.334	0.050	0.451	0.070	0.590	0.739	0.407	0.103	0.492	0.338	0.301	1.000	0.737	0.755	0.484	0.366	0.242
V	0.879	0.655	0.664	0.485	0.292	0.118	0.730	0.325	0.106	0.310	0.224	0.684	0.298	0.518	0.605	0.459	0.453	0.616